AWARD NUMBER: W81XWH-11-2-0071

TITLE: The Importance of Neurogenic Inflammation in Blast-Induced Neurotrauma

PRINCIPAL INVESTIGATOR: Michele L. Schaefer, Ph.D.

CONTRACTING ORGANIZATION: Johns Hopkins University
Baltimore, MD 21205

REPORT DATE: January 2013

TYPE OF REPORT: Annual

PREPARED FOR: U.S. Army Medical Research and Materiel Command
Fort Detrick, Maryland 21702-5012

REPORT DOCUMENTATION PAGE

Form Approved
OMB No. 0704-0188

1. REPORT DATE	2. REPORT TYPE	3. DATES COVERED
January 2013	Annual	1 January 2012 – 31 December 2012

4. TITLE AND SUBTITLE

The Importance of Neurogenic Inflammation in Blast-Induced Neurotrauma

5a. CONTRACT NUMBER

5b. GRANT NUMBER
W81XWH-11-2-0071

5c. PROGRAM ELEMENT NUMBER

6. AUTHOR(S)

Michele L. Schaefer, Ph.D.

E-Mail: michele.schaefer@jhuapl.edu

5d. PROJECT NUMBER

5e. TASK NUMBER

5f. WORK UNIT NUMBER

7. PERFORMING ORGANIZATION NAME(S) AND ADDRESS(ES)

Johns Hopkins University
Baltimore, MD 21205

8. PERFORMING ORGANIZATION REPORT NUMBER

9. SPONSORING / MONITORING AGENCY NAME(S) AND ADDRESS(ES)
U.S. Army Medical Research and Materiel Command
Fort Detrick, Maryland 21702-5012

10. SPONSOR/MONITOR'S ACRONYM(S)

11. SPONSOR/MONITOR'S REPORT NUMBER(S)

12. DISTRIBUTION / AVAILABILITY STATEMENT
Approved for Public Release; Distribution Unlimited

13. SUPPLEMENTARY NOTES

14. ABSTRACT

Scope: This project addresses the hypothesis that, in response to blast, blood-borne immune cells along with their secreted cytokines and chemokines from the periphery migrate via blood and infiltrate the CNS where they contribute to neuronal damage caused by activated microglia both in acute and chronic injury phases of blast-induced neurotrauma (BINT). To address the scientific feasibility of the hypothesis, we use state-of-the-art imaging and molecular techniques in mice with mild/moderate blast injury generated in a compressed helium-driven shock tube, throughout a one-month observation period. **Progress & Results:** At assigned time points after injury separate groups of animals with mild/moderate BINT are imaged by magnetic resonance imaging (MRI) to visualize potential macrophage infiltration; blood-brain barrier (BBB) disturbance; reactive gliosis; or astrocyte activation. The imaging findings were validated by immunocytochemistry. The obtained data suggest that a single exposure to mild/moderate blast induces both acute and chronic glial activation, levels of cytokines/chemokines, and motor impairment.

15. SUBJECT TERMS
blast, traumatic brain injury, brain, inflammation, magnetic resonance imaging, mice

16. SECURITY CLASSIFICATION OF:			17. LIMITATION OF ABSTRACT	18. NUMBER OF PAGES	19a. NAME OF RESPONSIBLE PERSON
a. REPORT	b. ABSTRACT	c. THIS PAGE			USAMRMC
U	U	U	UU	41	19b. TELEPHONE NUMBER *(include area code)*

Table of Contents

Introduction

Blast-induced neurotrauma (BINT), i.e., brain injury caused by blast exposure, causes the overwhelming majority of battlefield traumatic brain injuries (Owens, Kragh et al. 2008). Increased effectiveness of body armor to protect against projectiles as well as improved quality of acute trauma care significantly increased the survival rate among service members with blast injuries. However, because of these improvements, more individuals are surviving the acute phase of injury, making the development of long-term effects possible. While moderate and severe traumatic brain injuries (TBI) are easily identified and aggressively treated, milder TBIs or concussions, previously thought insignificant, frequently remain undiagnosed. Recent studies suggest blast exposure may cause inflammation in the brain, which could lead to long-term neurological deficits. We believe that blast injury mobilizes and activates immune cells from systemic circulation, which then secrete cytokines and chemokines in the blood as well as migrate through blood and lymph and enter the brain through disturbed blood-brain barrier (BBB). These chemicals and cells, once in the brain, activate glia and/or worsen the neuronal damage caused by activated microglia both in acute and chronic phases of BINT. Among major challenges in defining the pathobiology of TBI-induced neurogenic inflammation is the morphological similarity between macrophages that originate from periphery and then enter the brain, and the activated resident microglia. Clarifying these mechanisms would significantly help in developing novel diagnostic tests that would be capable of identifying patients with a higher risk of developing long-term neurological problems, and in assessing disease progression and monitoring the success of therapeutic interventions. In this annual report we have utilized current live imaging methods (i.e. magnetic resonance imaging) that track: immune cells entering the brain from systemic circulation; identifies BBB leakage; and visualizes the distribution of activated microglia and reactive gliosis, e.g., hallmarks of the inflammation in the brain. We have used methods of neuropathology and molecular biology (i.e. protein expression) to validate the imaging findings. Furthermore we are trying to deconstruct injury mechanisms by assessing the contribution of the direct shock wave to the head versus shock wave to the torso on the immune response. The imaging and molecular analyses are compared with functional tests measuring motor performance, memory, and behavior.

Body

Aim #1 MRI Imaging of Macrophage Infiltration, BBB Disturbance, and Glial Response in Mice Exposed to Mild, Moderate, or Severe Blast Exposure (18 months-October 1, 2010 to March 31, 2012)

Overall, animals have been imaged over multiple time points in the Georgetown University Animal MRI Laboratory generating hundreds of images. Mice received Feraspin particles (task 1.1. and Fig. 1), gadolinium (task 1.2. and Fig. 2-4), or MnCl2 (task 1.3. and Fig. 5-7). Pre- and post-contrast images have been acquired for all mice and representative images are included here (Fig. 1-7).

Task 1.1. MRI imaging of macrophage infiltration using iron oxide (FeOx) particles as a contrast

In order to provide information regarding inflammation and macrophage infiltration related to the site of blast injury, iron oxide contrast agent was injected intravenously and animals were imaged. We anticipated that the contrast agent would undergo specific uptake by macrophages. Moreover, we predicted that the opening of the BBB would preclude exclusion of the FeOx particles from the brain, and an area of negative (i.e. darkening) T2 MRI contrast would be evident in BINT mice. FeOx particles of various sizes (10-30 nm hydrodynamic diameter), composition (e.g. P904 has a glucose derivative coating designed for macrophage imaging applications), and concentrations (500 to 1000 μmol iron/kg body weight) were injected intravenously at various timepoints before and after blast exposure. Post-blast injection of the Feraspin XS FeOx particles (18 nm mean hydrodynamic diameter) resulted in FeOx being taken up in the reticuloendothelial system primarily. We next obtained P904 FeOx particles with a special glucose derivative coating for macrophage uptake with the expectation that these would be better at allowing access of the product to macrophages present in territories which are less accessible (i.e. brain) than well-vascularized tissues such as the liver or spleen.

When using the P904 FeOx particles (18 nm mean hydrodynamic diameter), we observed areas of decreased contrast that was not evident in the pre-injection image (Fig.1). However, enhancement was non-specific with contrast present in both normal and injured animals. Thus, these iron particles can cross the BBB and enter the brain without being taken up by macrophages. To differentiate between infiltrating FeOx laden peripheral macrophages and resident macrophages that take up FeOx, animals were imaged over a period of days (several half-lives past FeOx blood resident time). Signal enhancement was detected early as expected and persisted for 24 hrs. There was no appearance of newly generated signal (i.e. FeOx laden infiltrating macrophages) after 24

hrs. In conclusion, significant in vitro and in vivo work will need to be done to optimize parameters further, which is beyond the scope of this proposal.

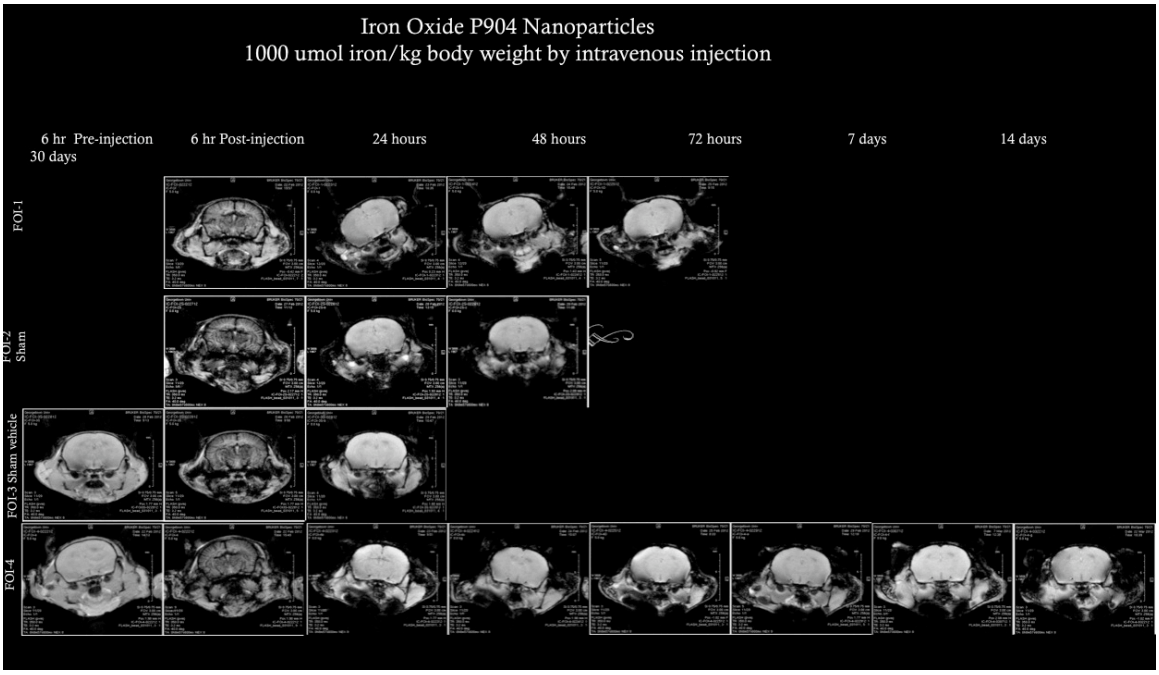

Figure 1 . Representative P904 FeOx enhanced MRI imaging. Passive diffusion of P904 was observed throughout the brain at 6 hrs post-injection. No obvious difference in signal enhancement was observed between injured and sham animals. Moderate blast injured brains (FOI-1, FOI-4). Sham brains (FOI-2S, FOI-3S). FLASH (fast low angle shot) imaging protocol was used with TR: 350 ms, TE: 3.2 ms, FOV: 3 cm, MTX: 256 and, 8 averages.

Task 1.2. MRI imaging of BBB disturbance using Gadofluorine M contrast agent.
Gadofluorine was not available and Gadolinium-DTPA (Gd-DTPI) was used as contrast in experiments intended to evaluate the BBB.

Multiple mice (Figs. 2, 3, and 4) were imaged using T1-weighted MRI before and after intraperitoneal (ip) injection with Gd-DTPI. Mice were imaged at 6 hr (pre-Gd) and 6 hr, 24 hr, 72 hr, 7 days, and 14 days, and 28 days post-Gd injection and blast.

Initial imaging experiments indicated there was a brightening of the brain in all scanned animals after the contrast administration (Figs. 2,3). While there was some day-to-day variability and variability between BINT animals they all seemed to trend toward increased brightening in the brain while sham treated animals had less contrast-uptake. These preliminary results were interpreted as the result of a compromised BBB. However, to confirm this finding signal would have to be normalized to eliminate day-to-day variability in signal intensity.

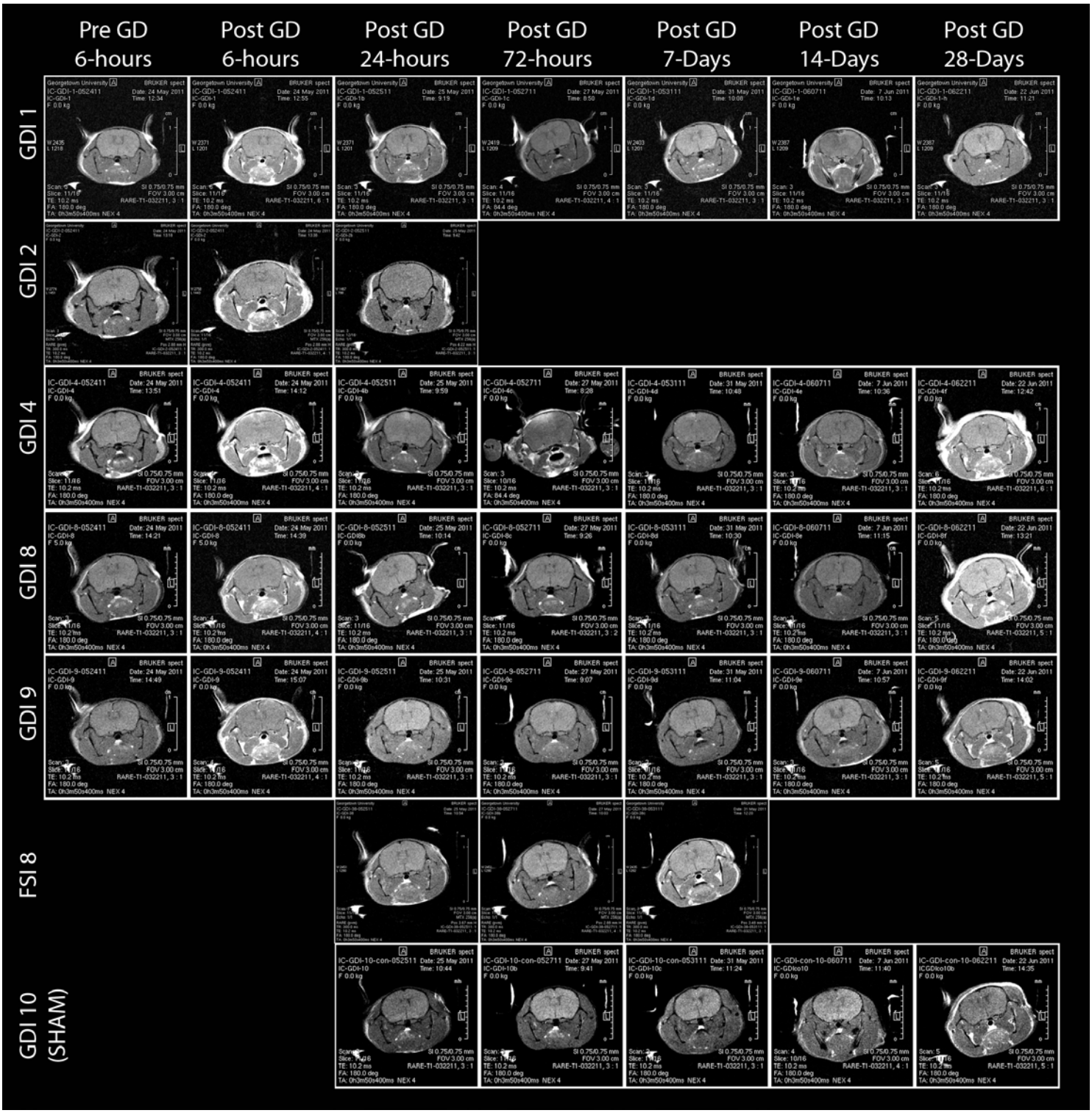

Figure 2 . Gadolinium T1 MRI Imaging: BBB disturbance. Animals imaged (BINT mice =GDI 1,2,4,8,9, and FSI 8; sham = GD1-10). The imaging protocol is: T1-weighted RARE with TR: 300 ms, TE: 10.2 ms, FOV: 3 cm, MTX: 256, averages: 4.

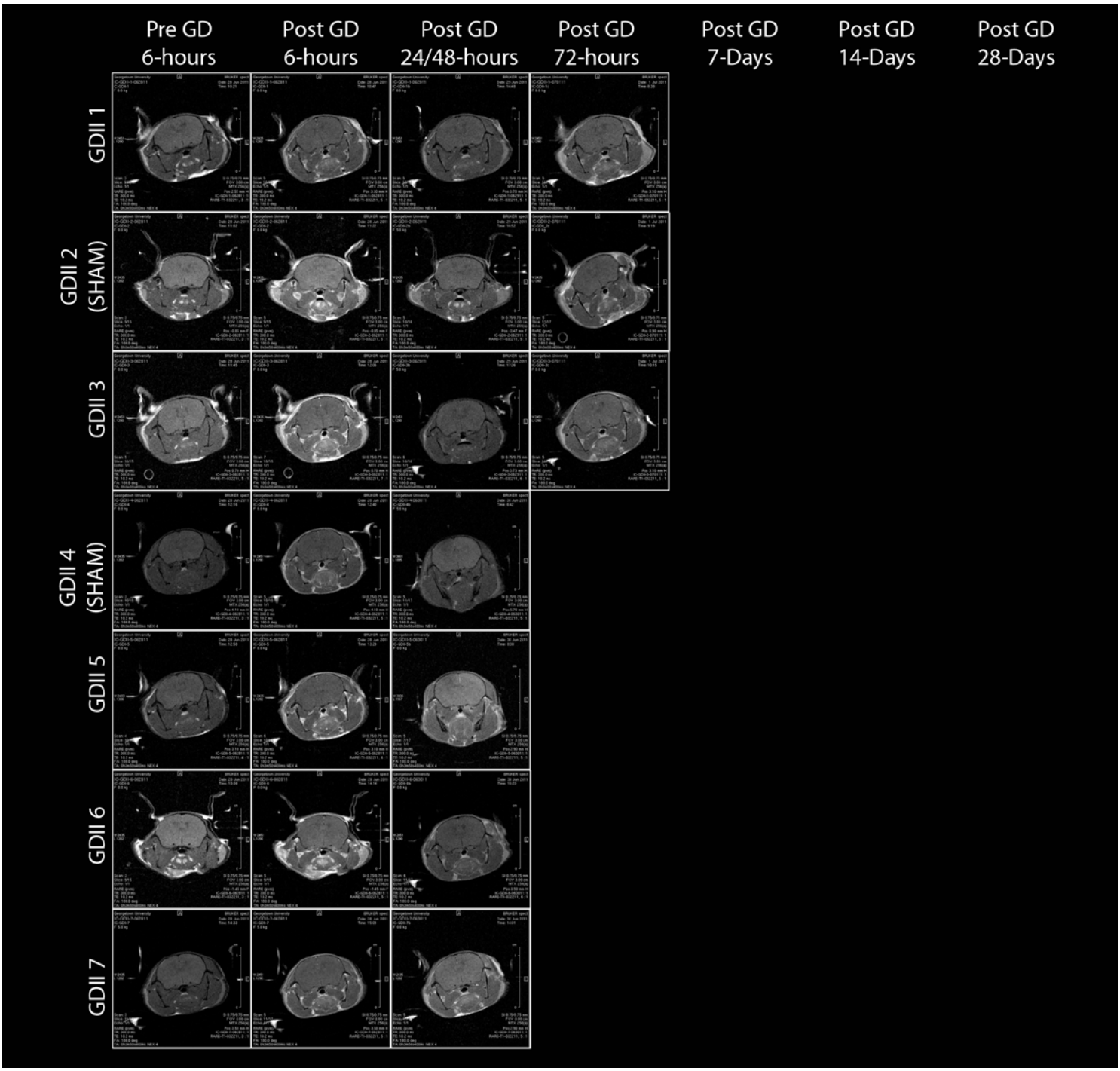

Figure 3. Gadolinium T1 Imaging: BBB disturbance. Animals imaged (BINT mice =GDII-1, 3 ,5,6, and 7; sham mice GDII-2 and GDII-4) The imaging protocol is: T1-weighted RARE with TR: 300 ms, TE: 10.2 ms, FOV: 3 cm, MTX: 256, averages:4

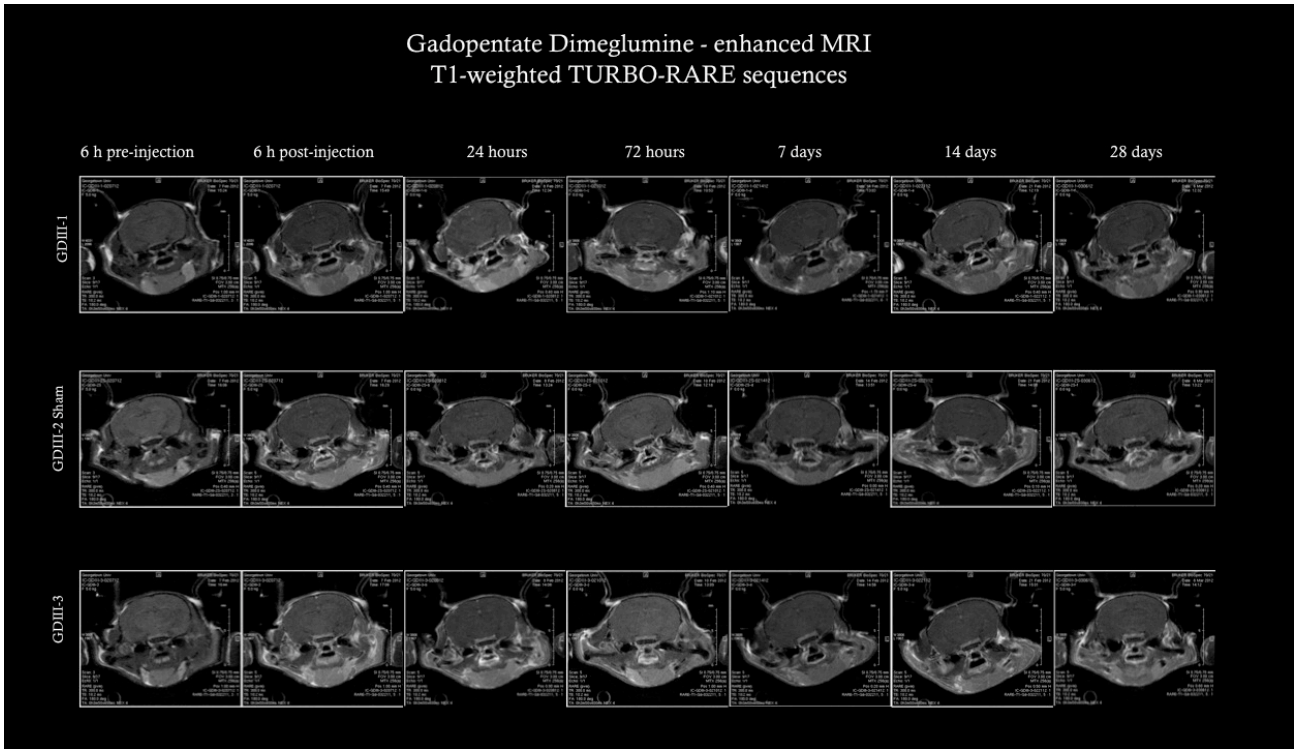

Figure 4. Gadolinium T1 MRI Imaging: BBB disturbance. Animals imaged (BINT mice = GDIII-1, and GDIII-3; sham = GDIII-2S). The imaging protocol is: T1-weighted RARE with TR: 300 ms, TE: 10.2 ms, FOV: 3 cm, MTX: 256, averages: 4.

With continued Gadolinium enhanced T1 MR imaging we were not able to reproduce the original findings (see Fig. 4 for example). We concluded that the signal enhancement occurs at or near the 'noise' level making interpretation difficult. Given that this contrast doesn't appear to be consistently enhancing signal in mild/moderate blast exposed animals we proposed to discontinue GD-DTPI imaging in our July 2012 quarterly report

Task 1.3. MRI imaging of reactive gliosis using $MnCl_2$- enhanced MRI (MEMRI)

Multiple animals were injected with the $MnCl_2$ neuronal contrast agent 24-hrs prior to BINT and were imaged with T1-weighted MRI (Figs. 5-6). MnCl2-induced signal enhancement was manifested by 48 hours and in some cases was followed by a gradual increase in signal in the area of the BINT.

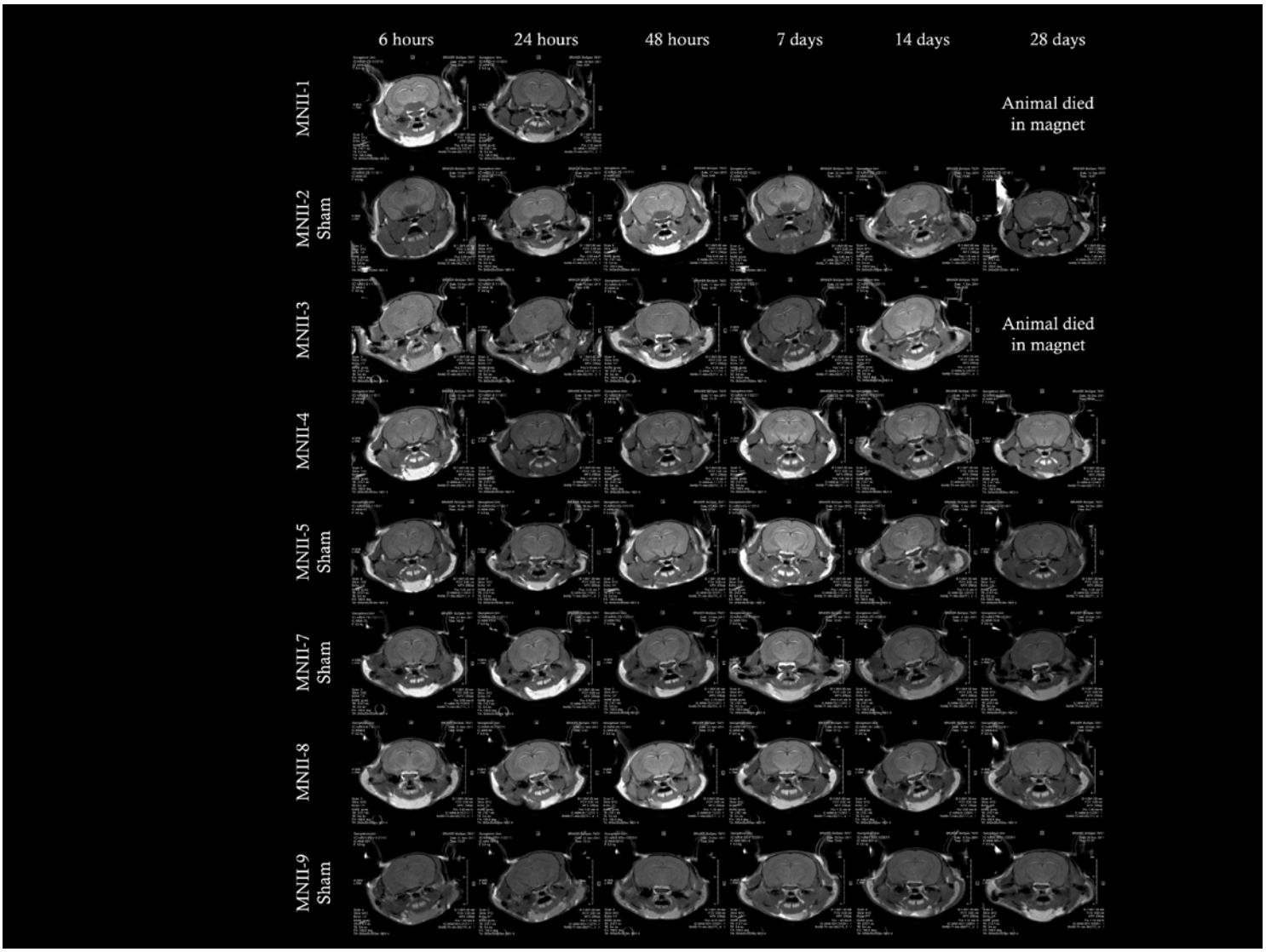

Figure 5. $MnCl_2$-enhanced T1 MRI: reactive gliosis. Animals (BINT mice = MNII 1, 3,4, 6, 8; sham = MNII 2, 5, 7 ,9). T1-weighted RARE (rapid acquisition with rapid enhancement) two-dimensional sequence with the following parameters: Matrix: 256, TR: 218.7 msec, TE: 9.4 msec, number of averages: 4, Rare factor: 1, FOV: 3.0 x 3.0 cm, number of slices: 12, slice thickness: 1 mm.

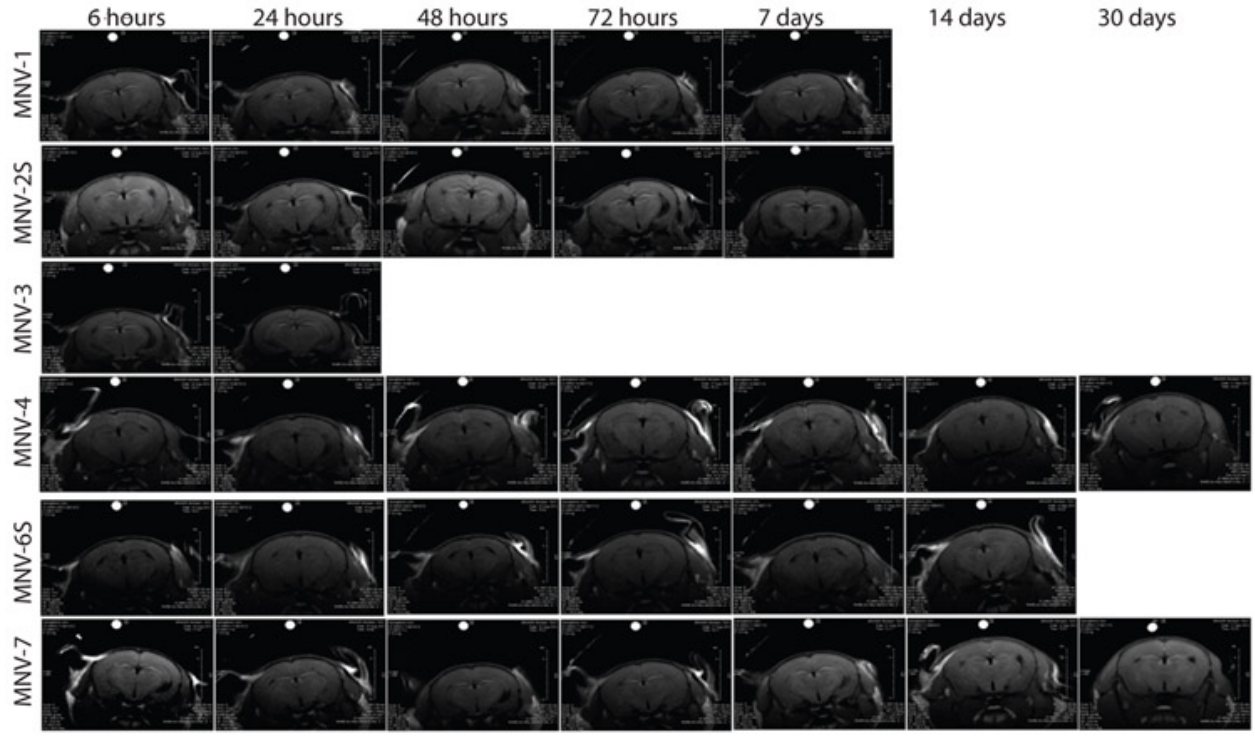

Figure 6. $MnCl_2$-enhanced T1 MRI: reactive gliosis. Animals (BINT = MNV-1, 3, 4, 7; sham = MNV-2S, 6S) Imaging Sequence, T1-weighted RARE (rapid acquisition with rapid enhancement) two-dimensional sequence with the following parameters: Matrix: 256, TR: 218.7 msec, TE: 9.4 msec, number of averages: 4, Rare factor: 1, FOV: 3.0 x 3.0 cm, number of slices: 12, slice thickness: 1 mm.

In summary, we chose to move forward with and optimize MnCl2-enhanced T1 MRI (see aim 4).

$MnCl_2$-T2 Imaging Control for Edema/Infarct

The purpose of the T2-weighted MRI in MnCl2-injected animals was to identify the presence of edema and hemorrhagic infarct. In all cases the animals were unremarkable and didn't show edema or infarcts (Fig. 7).

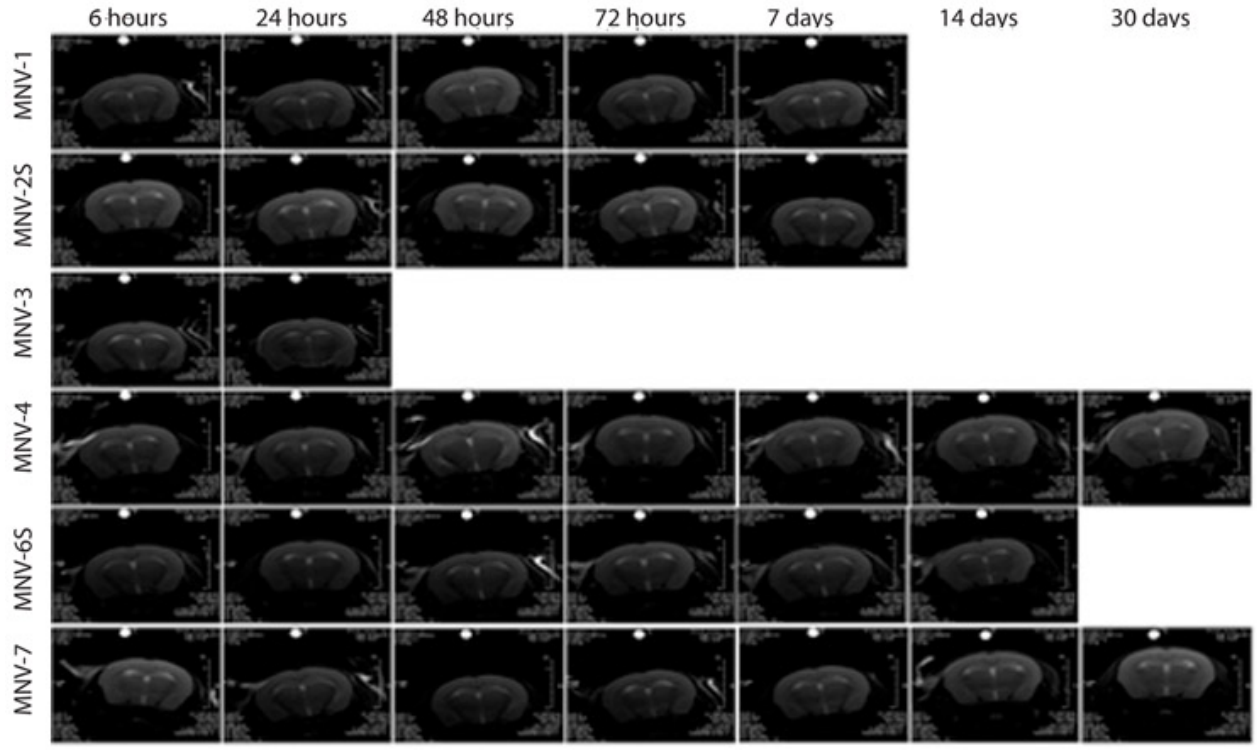

Figure. 7. Representative $MnCl_2$-enhanced T2-Weighted MRI: Imaging Edema and Hemorrhagic Infarct. Animals (BINT = MNV-1, 4, 7; sham MNV-2S, 6S). Imaging Sequence, T2-weighted RARE (rapid acquisition with rapid enhancement) two-dimensional sequence with the following parameters: Matrix: 256, TR: 4200 msec, TE: 12 msec, number of averages: 1, Rare factor: 8, FOV: 3.0 x 3.0 cm, number of slices: 12, slice thickness: 1 mm, and without respiratory gating to account for breathing movement.

Task1.4. In vivo bioluminescence imaging of activated astrocytes using GFAP-luciferase reporter mice

Twelve GFAP-luciferase reporter mice were imaged via the IVIS Spectrum camera at assigned time points (24 hr, 72 hr, 7 days, 14 days, 21 days, and 30 days) post-blast exposure (Fig. 8-10). The bioluminescent images were collected, standardized, normalized, and quantified. Overall, the luciferase bioluminescence suggests an astrocytic response is highest at the 24 hr time point and falls off rapidly by day 3 and continues to decline until reaching sham levels between days 7 and 14.

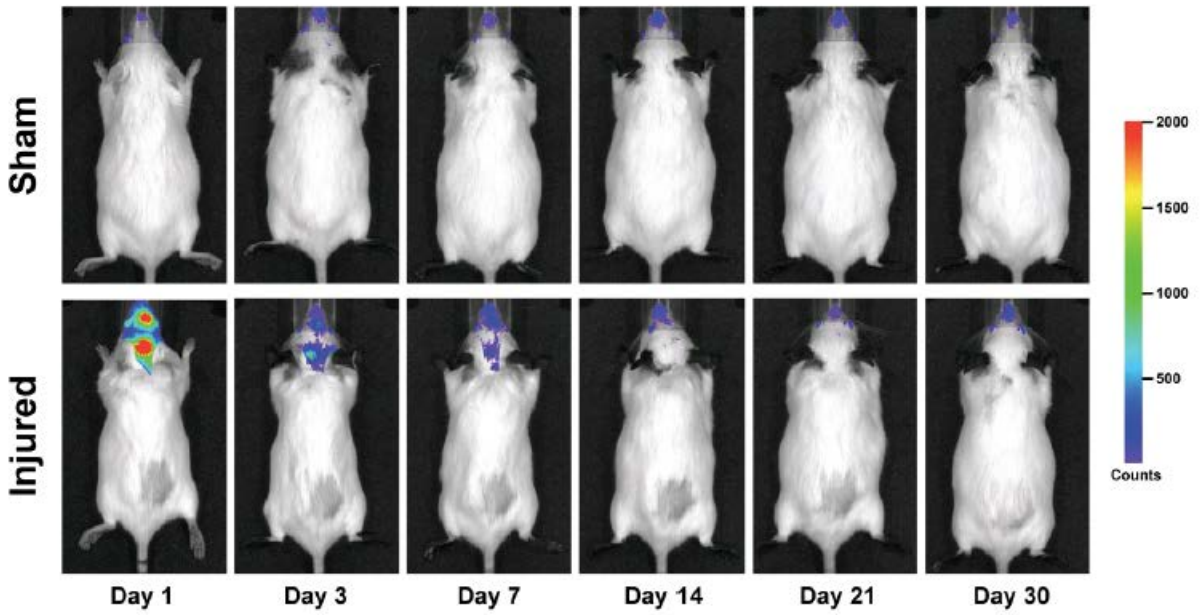

Figure 8. IVIS Imaging of luciferase bioluminescence in GFAP-luc transgenic mice – dorsal view. Sham and blast-exposed animal imaged (1, 3, 7, 14, 21, 30)

IVIS image series of quantitative bioluminescence (radiance flux –photons/second) emitted from the dorsal side of GFAP-Luc animals at specific time points (24h, 3d, 7d, 14d, 21d, 30d). Most artifactual regions of bioluminescence from transgenic animals (auto-bioluminescence in ears, foot-pads, tail) are removed, along with those from the Luciferin intraperitoneal injection (abdominal region). Autobioluminescence in these transgenic animals from the nose is not removed. Bioluminescence levels suggests that astrocytic response is highest at the 24h time point, falls off rapidly at days 3 and 7, and is comparable to sham bioluminescence levels at day 14 and after.

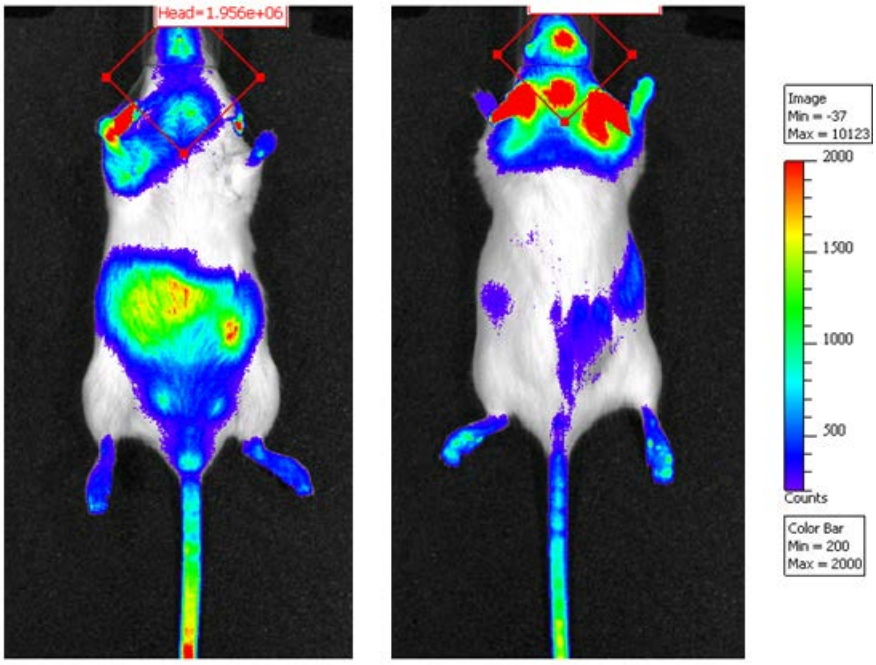

Figure 9. IVIS Imaging of Luciferase Bioluminescence – Region of Interest Definition
Ventral (left) and dorsal (right) images demonstrating the consistent definition of region of interest (ROI) summating the luciferase bioluminescence. This region considers the head and not the ears, which removes artifactual bioluminescence created from the GFAP-Luc transgenic mice that is emitted from the ears, footpads, and tail (that from the nose is not removed due to limited ROI shapes available and proximity to the olfactory system). This region of interest also removes radiance created from the Luciferin intraperitoneal injection (contrast visible on the abdomen of animal). For images display the ventral side of the animal, a region of interest (ROI) of 80 pixels by 80 pixels, at an angle of 45 to form a diamond shape is used. For images display the dorsal side of the animal, a region of interest (ROI) of 65 pixels by 65 pixels, at an angle of 45 to form a diamond shape is used. Ventral and dorsal images taken from injured animal at day 1 (open-field emission filter, 5 minutes).

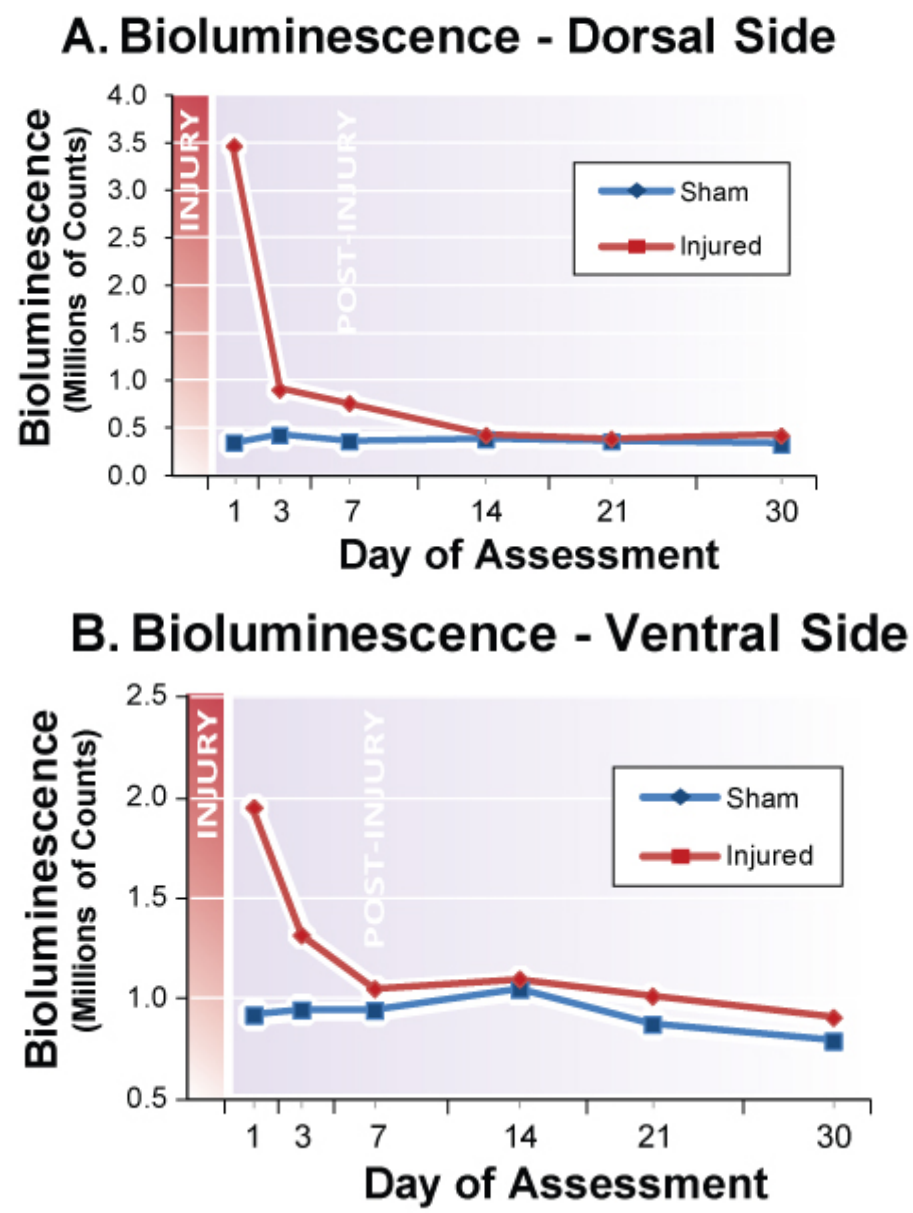

Figure 10. Quantitative luciferase bioluminescence captured in the ROI for dorsal (A) and ventral (B) images (total photon count summated at each pixel over 5 minute bioluminescence imaging period with no emission filter) of GFAP-Luc animals at specific time points (24h, 3d, 7d, 14d, 21d, 30d, Sham n=1, Injured n=1). Luciferase bioluminescence suggests astrocytic response is highest at the 24h time point, falls off rapidly at days 3 and 7, and is comparable to sham bioluminescence levels at day 14 and after.

Aim 2 (24 months – April 1, 2011 to March 31, 2013) Validation of imaging results by methods of neuropathology and molecular biology, and characterization of neurogenic inflammation due to blast

Tasks 2.1 – 2.2. Neuropathology and characterization of neurogenic inflammation using immunocytochemistry

Neuropathology

Two preliminary surveys, hemotoxylin and eosin (H&E) and Fluorojade staining, were performed to assess neurodegeneration in the brains of mice post mild/moderate blast (results presented in 1/31/12 annual report). Rare events were detected in a variety of brain regions at 7 and 14 days post blast. H&E showed a slight increase (~4x) in eosinophilic degenerating neurons in the anterior portion of the brain (including cingulate cortex, caudate putamen, and preoptic area of the hypothalamus). A slight increase in Fluorojade-C staining was observed in the fimbria and cingulum.

Immunohistochemistry

Thirty two mouse brains (18 experimental and 14 sham brains euthanized 24h, 3d, 7d, 14d, and 1 month after injury) were sectioned (40 µm), and stored in a cryoprotectant solution in -20 degrees for further processing. Microglia and astrocytes were labeled with an immunoperoxidase-DAB method using CD68 and IBA-1 antibodies for microglial labeling and GFAP for astrocyte labeling. Every 24th section starting from the beginning of cortex rostrally to the posterior edge of cerebellum caudally was picked up and processed as described (Sheng, Bora et al. 2003).

Immunocytochemistry with CD68 and IBA-1 antibodies demonstrates that mild-moderate blast injury causes microglial activation in various gray and white matter regions at all time points after blast. However, location of microglial activation varies among cases and time points. Densities of CD68 (+) and IBA-1 (+) microglia were estimated at these locations. CD68 and IBA-1(+) immunoreactivity in activated microglia overlapped substantially, a pattern confirming the presence of focal neuroinflammation in these areas (Table 1, Fig. 11). The visual system (optic tract, superior colliculus) and cerebellar folia were the regions most frequently involved, a pattern suggesting that mild-

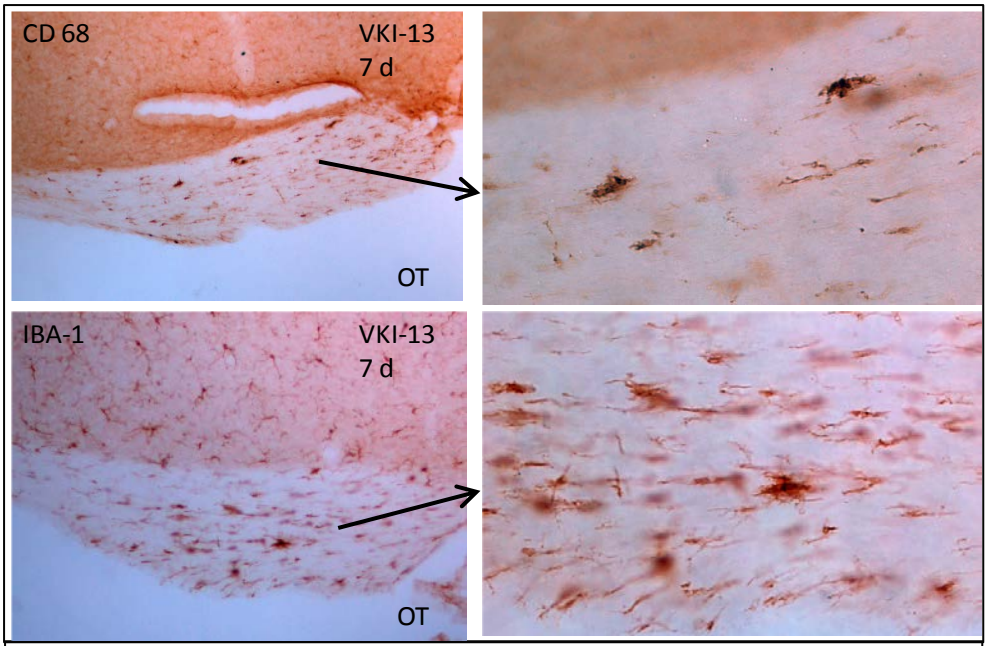

Figure. 11. In this case of a subject euthenized 7d after mild-moderate blast injury (VKI-13), microglia/macrophages are activated in the optic tract, as evidenced by CD 68 (left upper panel) and IBA-1 (left lower panel) immunoreactivity on adjacent sections. Right panels are enlarged to depict cellular detail.

moderate blast injury in mice has a propensity to affect the visual system and cerebellum (Table 1).

Table 1: Density of activated microglia/macrophages in various brain areas based on CD68 and IBA-1 immunoreactivity

		Frnx		Optic		LL		Hipp		Crbl folia		SuC		LG	
number	Time	CD68	IBA-1	CD68	IBA-1	CD68	IBA-1	CD68	IBA-1	CD68	IBA-1	CD68	IBA-1	CD68	IBA-1
VKI-24	24 hr	+	+					+							
VKI-19	24 hr							±	?						
VKI-9	72 hr			+	?	+						+++	+++	+++	?
VKI-20	72 hr														
VKI-19 (2)	7 day							+	±						
VKI-13	7 day			++	++					++	?				
VKI-28	30 day			+	+					+	+		±		
VKI-26	30 day			+	+					+	±				
VKI-22	30 day			+	+					±					

Abbreviations: Frnx, fornix; Optic, optic tract; LL, lateral lemniscus; Crbl folia, cerebellar folia; Hipp, hippocampus; SC, superior colliculus;LG, lateral geniculate neucleus
Note: Highlighted subject is the subject with contusion.

Except in the case of optic tract in some subjects, GFAP immunocytochemistry did not demonstrate substantial astrocytic activation in injured mice (Fig. 12).

A contusion in the frontal cortex was present in two cases (VK1-9 and L3). The contusion area was strongly positive for all three markers used (CD68, IBA-1 and GFAP) (Fig. 13).

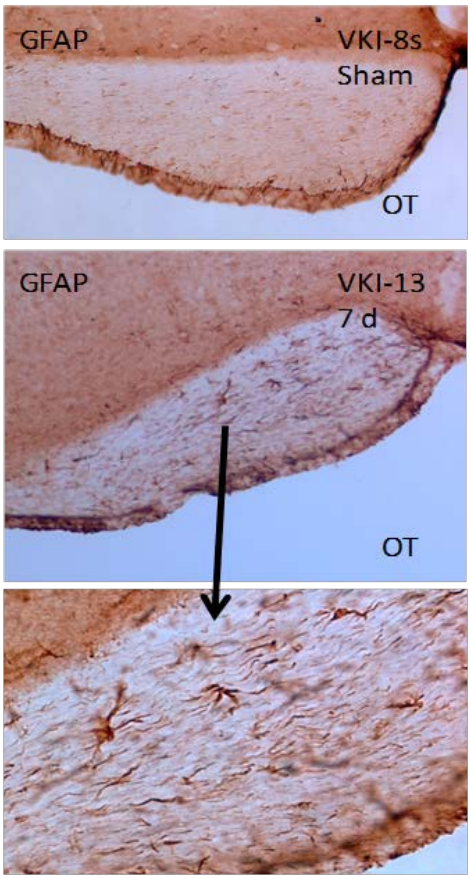

Figure 12.. In this case 7d after mild-moderate blast injury (VKI-13), there was astrocytic activation in the optic tract based on GFAP immunoreactivity (compare experimental subject in middle panel with sham control [VKI-8s] on top). Bottom panel is an enlargement of indicated region in middle panel to show cytological detail.

These findings suggest that mild-moderate blast exposure can cause focal neuroinflammation. However, the temporal and spatial dynamics of neuroinflammation are unclear because of the variance in density and location of activated microglia at various time points after blast injury. In addition, the role and type of microglia/macrophages in this type of neuroinflammation needs to be ascertained.

In the last quarter, additional cases have been processed including another time point (at 2 weeks). These cases are being counted, so that we have a full picture of these changes.

Immunocytochemistry with IBA-1 antibody demonstrates that mild/moderate blast injury at 2 weeks causes microglial activation in the gray and white matter in patterns resembling other time points mentioned above (Fig. 14). Densities of activated microglia (hypertrophic or bushy IBA1(+) morphologies were estimated at several locations (Table 2). The visual system (optic tract, superior colliculus) and cerebellar folia were the region's most frequently involved, a pattern suggesting that mild/moderate blast injury in mice has a propensity to primarily affect the visual system and cerebellum (Table 2).

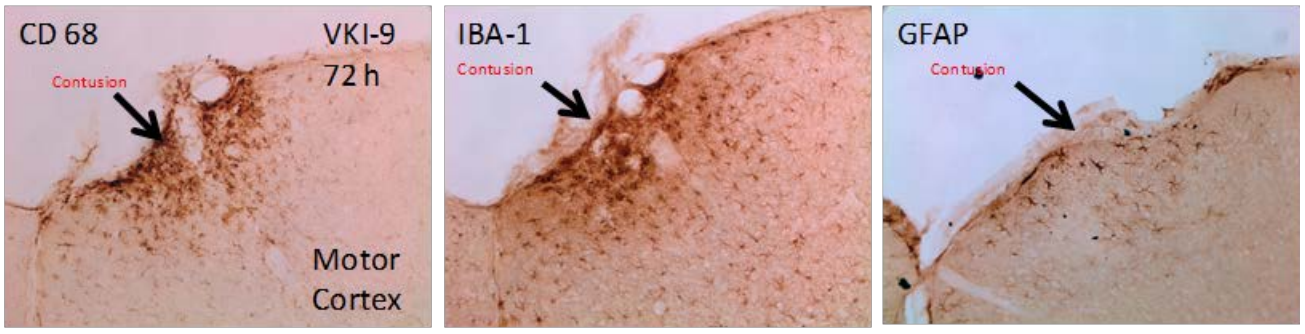

Figure 13. In this case of a subject sacrificed 72h after mild/moderate blast injury (VKI-9), microglia is activated in the contusion area of motor cortex (arrow). Right panel depicts intensely GFAP-immunoreactive astrocytes in the same area.

Departing from previous reports, a few new cases showed activated IBA-1 (+) profiles in lower corpus callosum and immediately adjacent sub-callosal regions (Fig. 15 , Table 2).

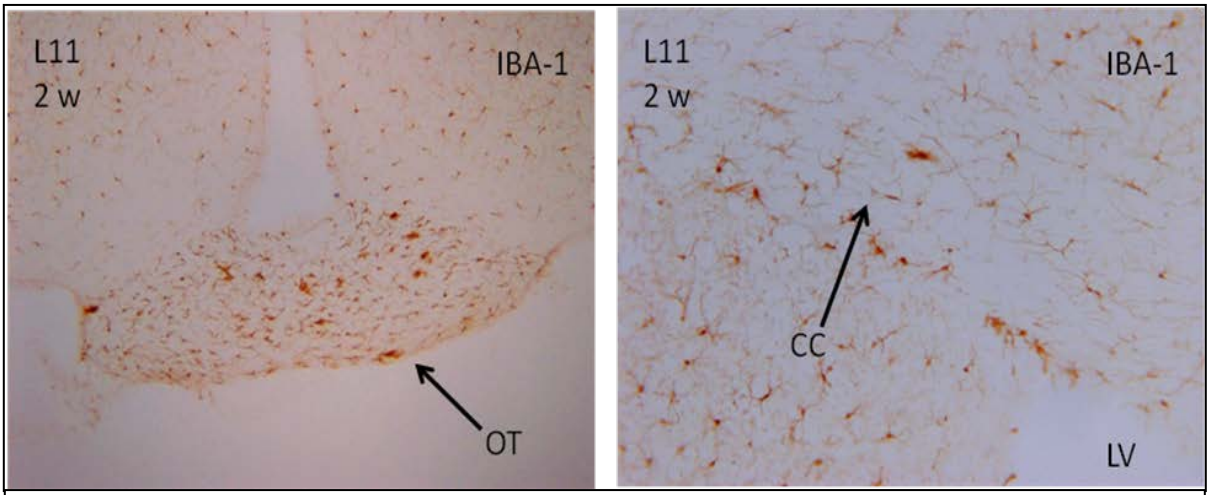

Figure 14. In this case of a subject euthenized 2 weeks after mild-moderate blast injury (L11), microglia/macrophages are activated in the optic tract (chiasm) and corpus callosum, as evidenced by IBA-1 immunoreactivity.

Activated IBA-1(+) microglial profiles are being counted in the optic tract with stereology. Counts have been completed for one case per time point. Results show that neuroinflammation in the optic tract gradually increased from 24 hours to 2 weeks and then decreased at 30 days after mild-moderate blast injury (Fig. 16).

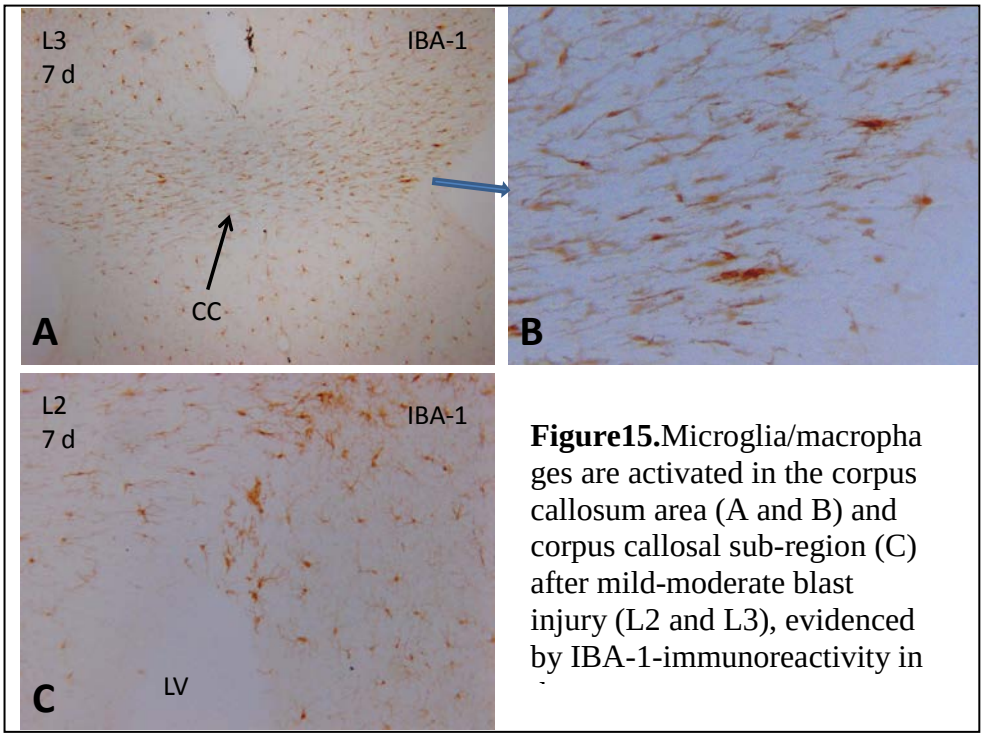

Figure15. Microglia/macrophages are activated in the corpus callosum area (A and B) and corpus callosal sub-region (C) after mild-moderate blast injury (L2 and L3), evidenced by IBA-1-immunoreactivity in

These initial findings suggest that mild-moderate blast exposure causes focal neuroinflammation in the visual system and cerebellum. The temporal and spatial dynamics of neuroinflammation in the visual system will be definitely characterized when counts for activated microglia are completed.

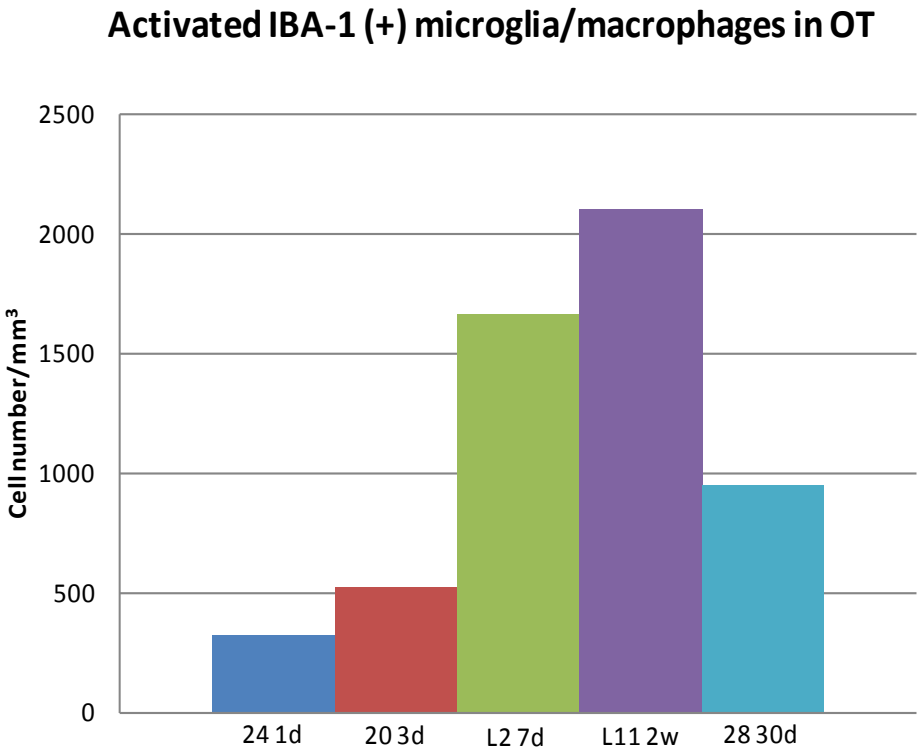

Figure 16. Temporal profile of activated microglia/macrophages in the olfactory tract

Table 2 : Density of activated microglia/macrophages in various brain areas based on IBA-1 immunoreactivity

		Frnx	OT	CC	Hipp	Crbl	SuC	LG	SN	PY
L2	7 d		++	+	±	+	±		+	
L3	7 d		++	++		+	++	+		
L4	7 d		++	++	+		+	++		
L5	2 w		+						+	
L7	2 w	±	+			+				+
L9	2 w			±		+				+
L11	2 w		+++	+			±	+		
LXU2-1	30 d					±				

Abbreviations: Frnx, fornix; Optic, optic tract; LL, lateral lemniscus; Crbl folia, cerebellar folia; Hipp, hippocampus; SuC, supper colliculus;LG, lateral geniculate body; SN, septal nucleus; PY, pyramidal tract

Note: Highlighted subject is the subject with contusion.

Task 2.3 Task has not yet been attempted.

Task 2.4 Results of this task have been published (see Fig 9-11 in Cernak, Merkle et al. 2011).

Task 2.5 Measuring cytokine and chemokine protein expression using immunoassays

It is generally believed that primary blast shock waves can result in neuroinflammation in the brain. During the acute phase response, immune cells secrete pro-inflammatory cytokines (e.g. TNF-α, IL1-β, IFNγ, IL6) which further recruit hematogenous immune cells. The response is propagated by release of chemokines which recruit even more immune cells to the area. As a result of this massive immune infiltration large amounts of cytotoxic cytokines are produced which prolong injury. Added on top of this is a complex interaction between the gut and brain. After injury, systemic immune cells, chemicals (e.g. cytokines and chemokines), and vagus nerve stimulation can have an effect on the brain. Previous results from our laboratory showed that shielding of the torso (but not head protection) dramatically reduces inflammation in the gut and brain (Cernak 2010) and ameliorates axonal injury and behavioral deficits (Koliatsos, Cernak et al. 2011). These results suggest a robust influence of the gut immune and vagus nervous system on the brain following blast trauma to the torso.

During the past two quarters we have generated preliminary data supporting a systemic role in blast-induced neurotrauma. We compared expression of a variety of cytokines, chemokines, and growth factors in dissected brain tissue and blood (Figs. 17-23) and spleen (Fig. 24) in blast exposed animals with and without shielding. We are picking up some interesting differences between torso protected animals and head protected or shams.

Notably, in all samples tested we see a large difference in CXCL1 (GRO-α) expression between torso protected animals and head protected or shams at the 30 day post trauma period (chronic period; see Figure 4). CXCL1, a small cytokine expressed by neurons, macrophages, neutrophils, and endothelial cells, has been shown to have neuroprotective functions and can induce proliferation and inhibit migration of oligodendrocytes. Importantly, CXCL1 has been shown to attenuate microglial activation and maintain them in a quiescent state (Lyons, 2009). It will be interesting to investigate whether shielding of torso and thus increased CXCL1 levels modulates microglial activation state.

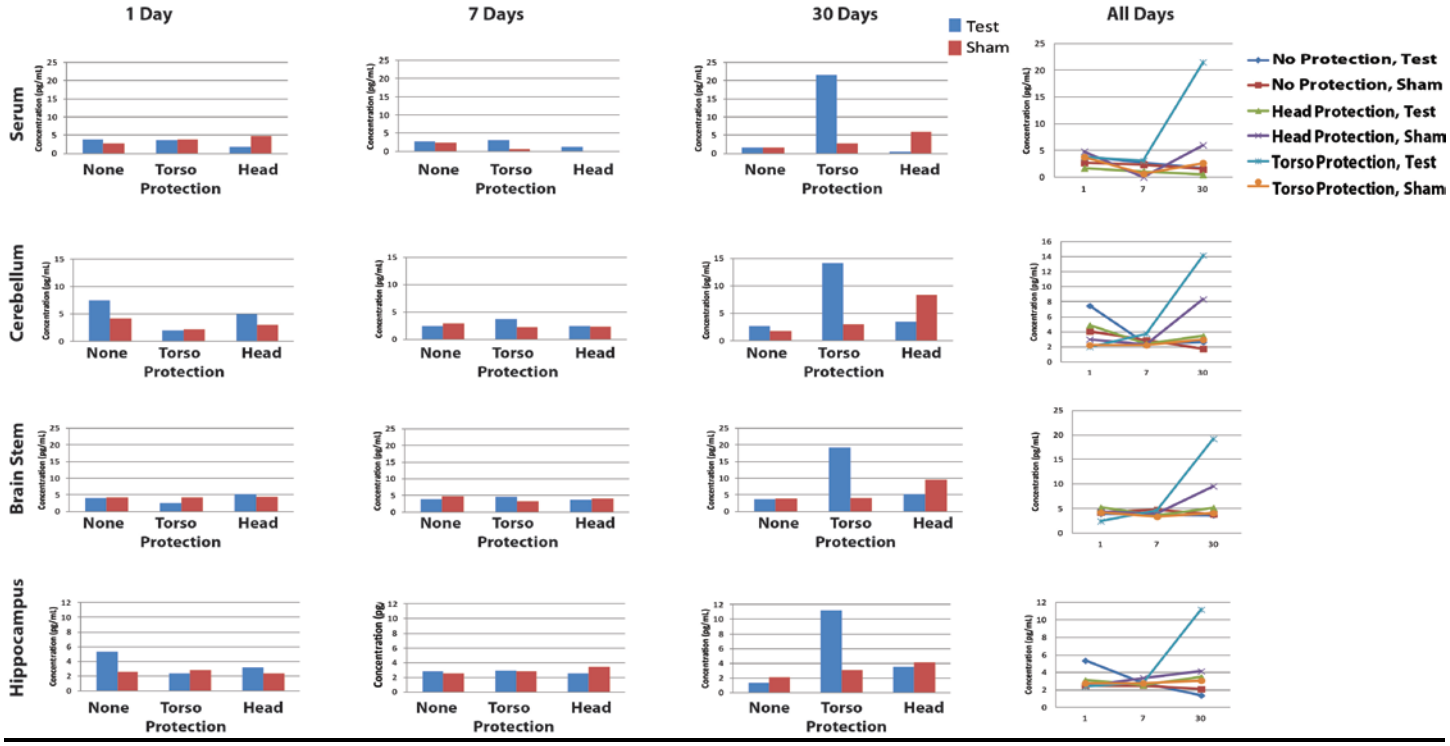

Figure 17 Temporal protein expression levels of Gro-α (CXCL1) in mice with and without protective wear and exposure to blast. Individual sample types are plotted in rows (serum, cerebellum, brain stem, and hippocampus). The time post injury is plotted in columns (1, 7, and 30 days post-blast). The blue bars represent the injured animals and the red bars are the sham controls. The last column is depicting the evolving data over the 30-day period. The y-axis represents the concentration in pg/ml.

We see approximately 4-fold higher levels of G-CSF in the serum of torso protected animals (Fig. 18). G-CSF is a growth factor and cytokine that can act on neuronal cells as a neurotrophic factor. The action of G-CSF in the CNS is to induce neurogenesis, to increase neuroplasticity and to counteract apoptosis. These properties are currently under investigation for the development of treatment of neurological diseases such as cerebral ischemia.

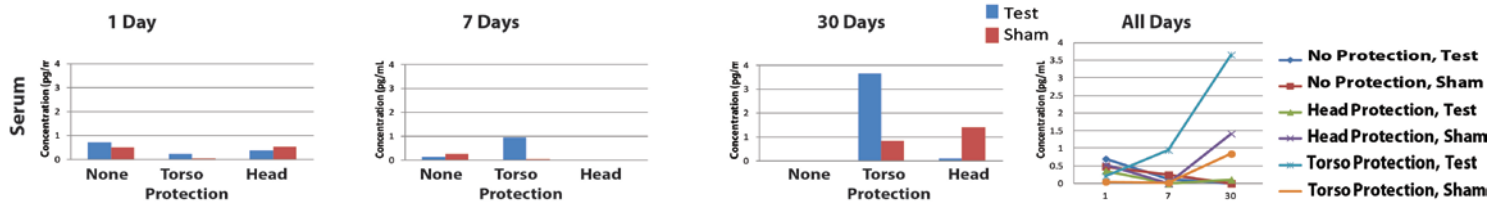

Figure 18 Temporal protein expression levels of G-CSF in mice with and without protective wear and exposure to blast. Individual sample types are plotted in rows (serum, cerebellum, brain stem, and hippocampus). The time post injury is plotted in columns (1, 7, and 30 days post-blast). The blue bars represent the injured animals and the red bars are the sham controls. The last column is depicting the evolving data over the 30-day period. The y-axis represents the concentration in

pg/ml.

Increased levels of IL-6 are also seen in the serum and spleen at 30 post injury in the torso protected animals (Figures 19 and 24). IL-6 acts as both a pro-inflammatory and anti-inflammatory cytokine. Its role as an anti-inflammatory cytokine is mediated through its inhibitory effects on TNF-α and IL-1, and activation of IL-1ra and IL-10. IL-6 is capable of crossing the blood brain barrier (as are many cytokines and chemokines). Synthesis of IL-6 can be induced by CXCL-1.

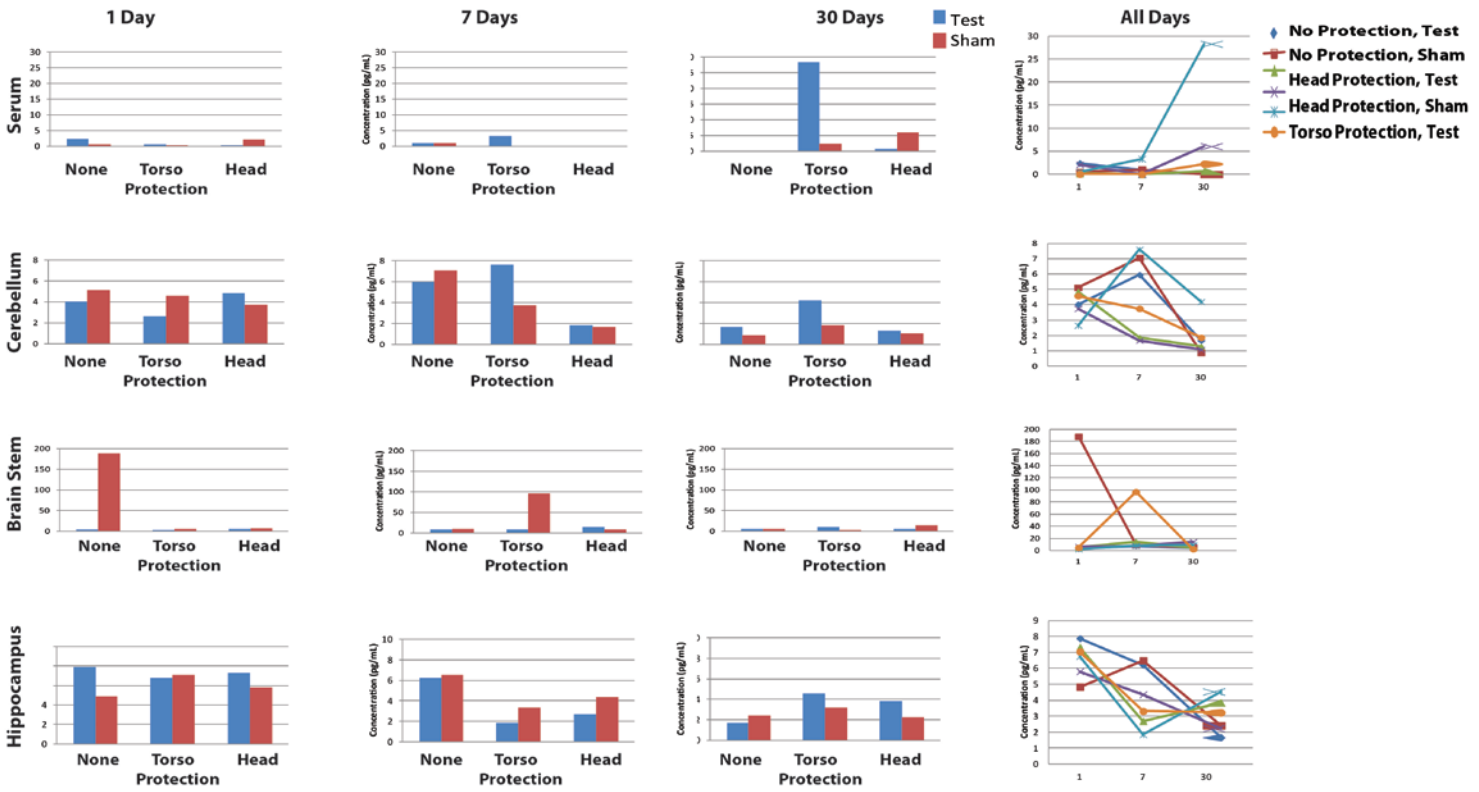

Figure 19 Temporal protein expression levels of IL-6 in mice with and without protective wear and exposure to blast. Individual sample types are plotted in rows (serum, cerebellum, brain stem, and hippocampus). The time post injury is plotted in columns (1, 7, and 30 days post-blast). The blue bars represent the injured animals and the red bars are the sham controls. The last column is depicting the evolving data over the 30-day period. The y-axis represents the concentration in pg/ml.

Fewer differences were detected in VEGF-A, TNF-α, IL1-β, and IL-10 (figures 20-23).

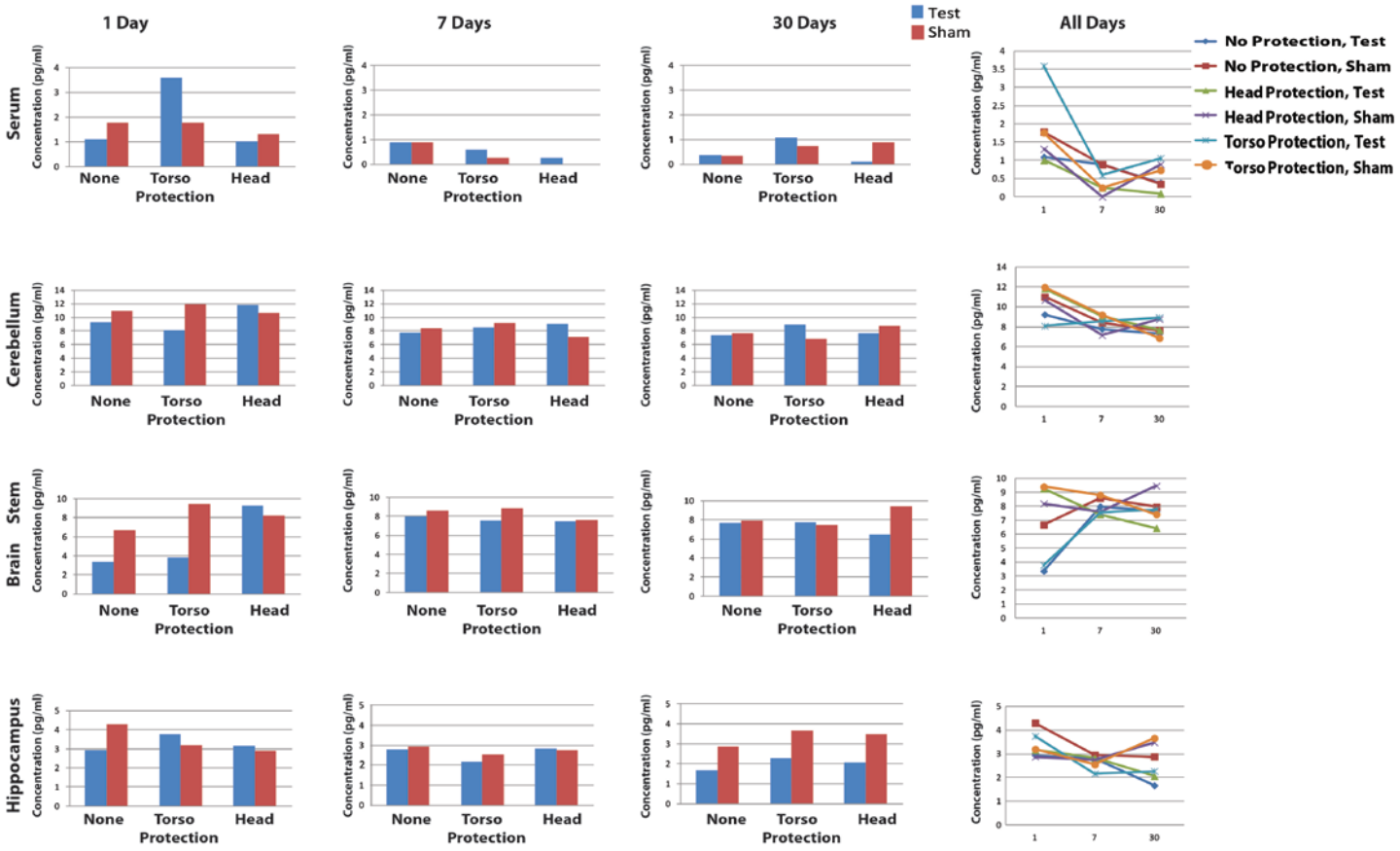

Figure 20 Temporal protein expression levels of VEGF-A in mice with and without protective wear and exposure to blast. Individual sample types are plotted in rows (serum, cerebellum, brain stem, and hippocampus). The time post injury is plotted in columns (1, 7, and 30 days post-blast). The blue bars represent the injured animals and the red bars are the sham controls. The last column is depicting the evolving data over the 30-day period. The y-axis represents the concentration in pg/ml.

VEGF-A appears slightly elevated in the serum. VEGF-A has been shown to be expressed by inflammatory cells (e.g. polymorphonuclear leukocytes) and astrocytes. It can be stimulated by hypoxic conditions and inhibited by edema and necrosis (Nag, Eskandarian et al. 2002). It mediates vascular permeability (vasodilator), induces angiogenesis, vasculogenesis, endothelial cell growth, cell migration, and can inhibit apoptosis. Importantly, VEGF, a HIF-1α target gene is known to play a critical role in the early phase after different forms of brain injury by causing BBB disruption leading to cerebral edema (Nag, Takahashi et al. 1997; Zhang, Zhang et al. 2000; Fagan, Hess et al. 2004; Jadhav, Matchett et al. 2007).

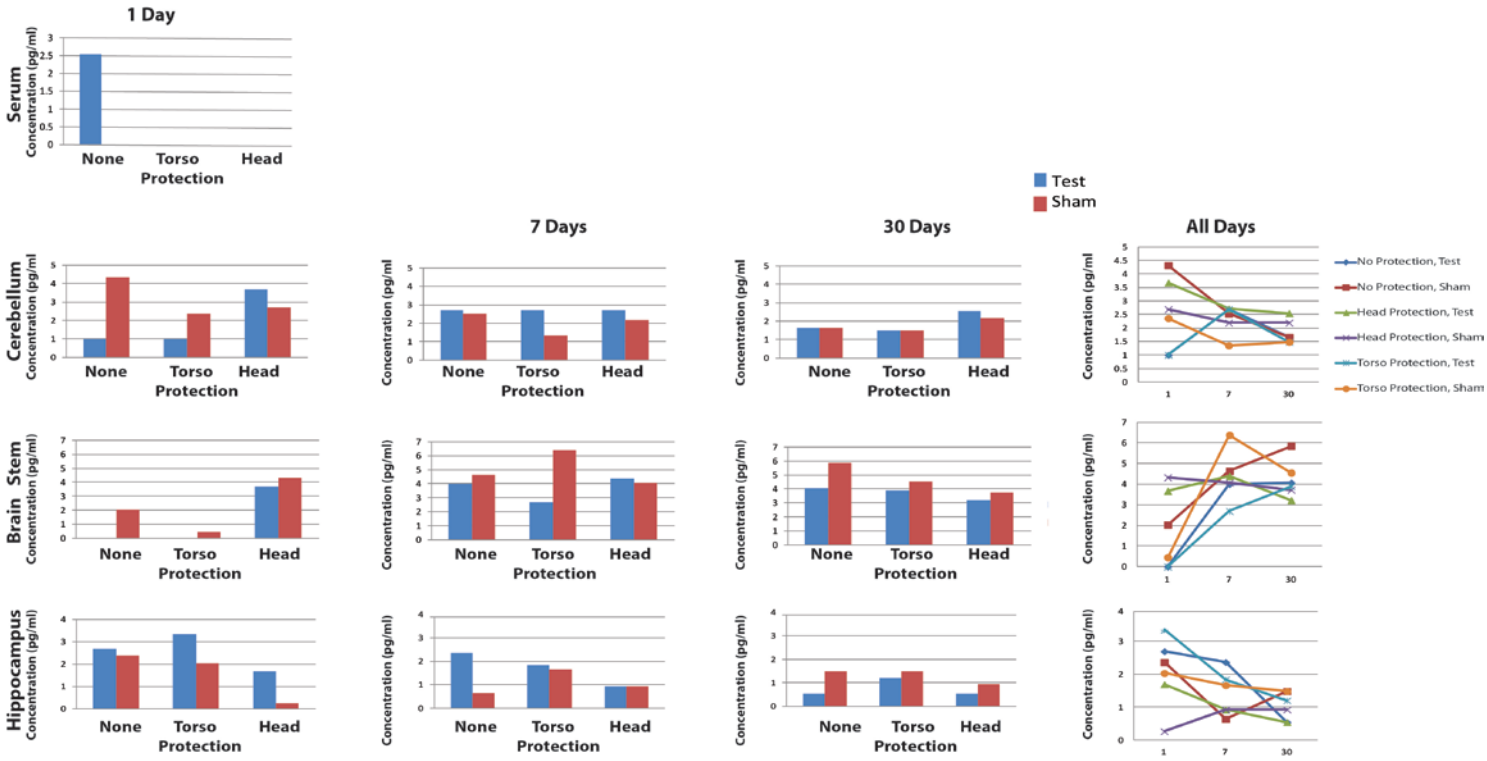

Figure 21 Temporal protein expression levels of TNF-α in mice with and without protective wear and exposure to blast. Individual sample types are plotted in rows (serum, cerebellum, brain stem, and hippocampus). The time post injury is plotted in columns (1, 7, and 30 days post-blast). The blue bars represent the injured animals and the red bars are the sham controls. The last column is depicting the evolving data over the 30-day period. The y-axis represents the concentration in pg/ml.

As expected, there is an increase in TNF-α in the acute phase of the injury response in the serum.

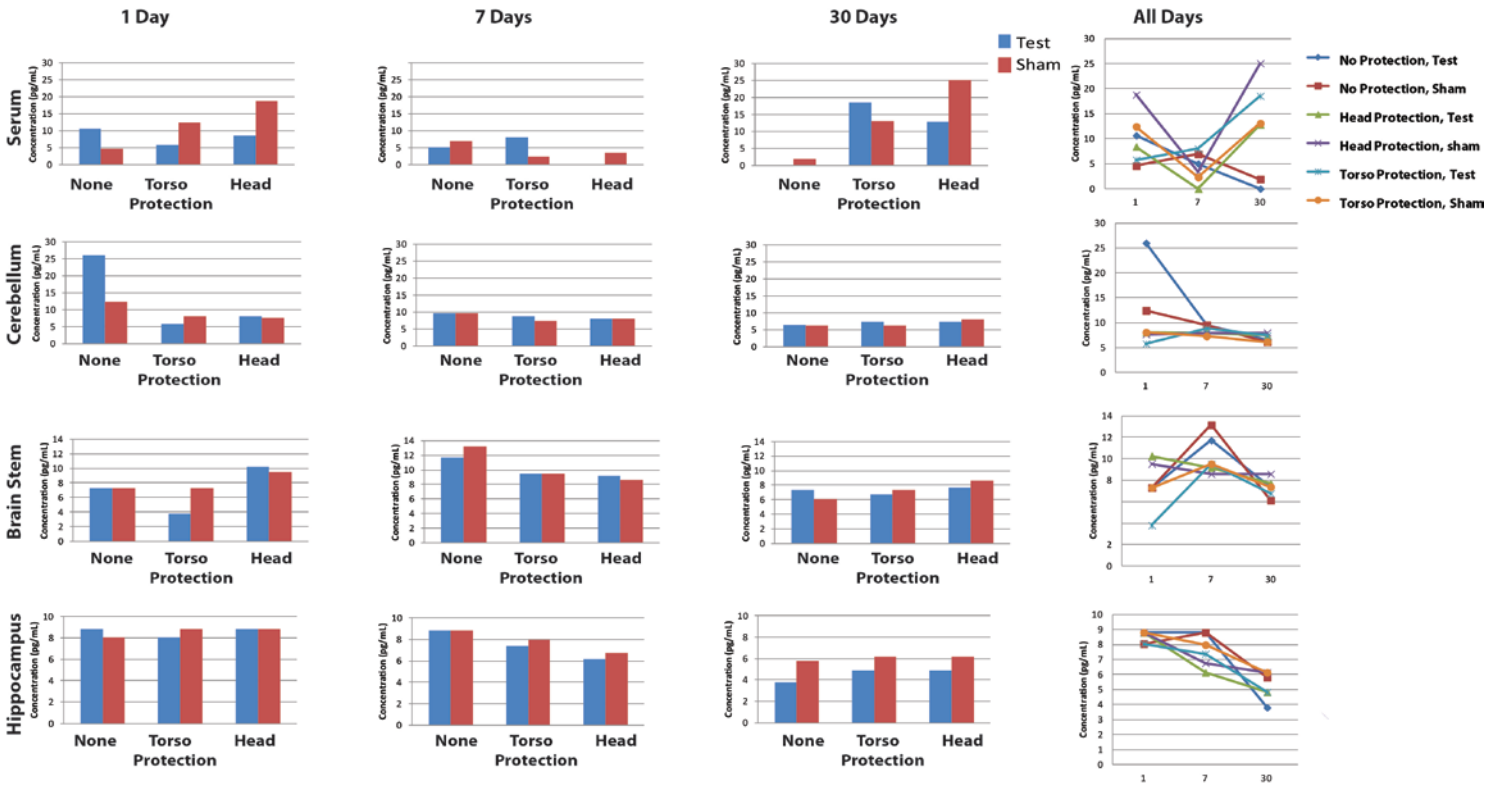

Figure 22 Temporal protein expression levels of IL1-β in mice with and without protective wear and exposure to blast. Individual sample types are plotted in rows (serum, cerebellum, brain stem, and hippocampus). The time post injury is plotted in columns (1, 7, and 30 days post-blast). The blue bars represent the injured animals and the red bars are the sham controls. The last column is depicting the evolving data over the 30-day period. The y-axis represents the concentration in pg/ml.

There appears to be an increase in IL1-β cerebellum of injured mice. IL1-β is a member of the interleukin 1 cytokine family produced by activated macrophages as a proprotein, which is proteolytically processed to its active form by caspase 1 (CASP1/ICE). It is an important mediator of the inflammatory response, and is involved in a variety of cellular activities, including cell proliferation, differentiation, and apoptosis. The induction of cyclooxygenase-2 (PTGS2/COX2) by this cytokine in the central nervous system (CNS) is found to contribute to inflammatory pain hypersensitivity.

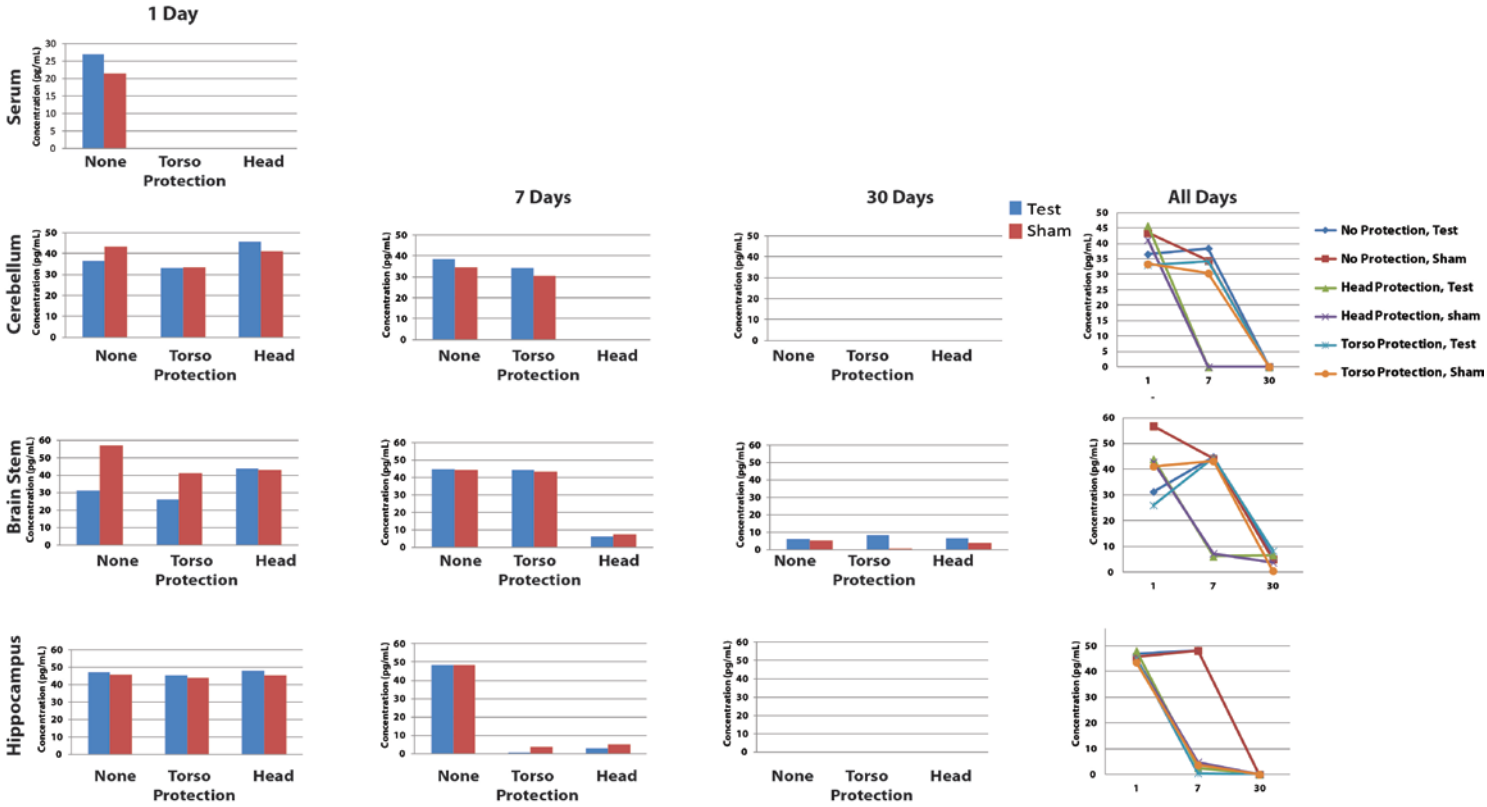

Figure 23 Temporal protein expression levels of IL-10 in mice with and without protective wear and exposure to blast. Individual sample types are plotted in rows (serum, cerebellum, brain stem, and hippocampus). The time post injury is plotted in columns (1, 7, and 30 days post-blast). The blue bars represent the injured animals and the red bars are the sham controls. The last column is depicting the evolving data over the 30-day period. The y-axis represents the concentration in pg/ml.

IL-10 expression did not appear to be significantly different between sham and injured or any of the groups in Fig. 10. It is unclear why this interleukin is expressed in both sham and injured animals acutely and then wanes over the 30-day period. It is likely this measurement is confounded by the isoflurane anesthesia used during vitals measurements and during injury induction. IL-10 is slightly increased in the spleen of all injured groups at 30-days post injury (data not shown). IL-10 is an anti-inflammatory cytokine with pleiotropic effects in immunoregulation and inflammation. IL-10 can block NF-KB activity. Knockout studies in mice suggested the function of this cytokine as an essential immunoregulator in the intestinal tract; and, indeed, patients with Crohn's disease react favorably towards treatment with recombinant interleukin-10-producing bacteria, demonstrating the importance of IL-10 for counteracting the hyperactive immune response in the human body. IL-10 is capable of inhibiting synthesis of pro-inflammatory cytokines such as IFN-g, IL-2, IL-3, TNFα, and GM-CSF made by cells such as macrophages and regulatory T-cells

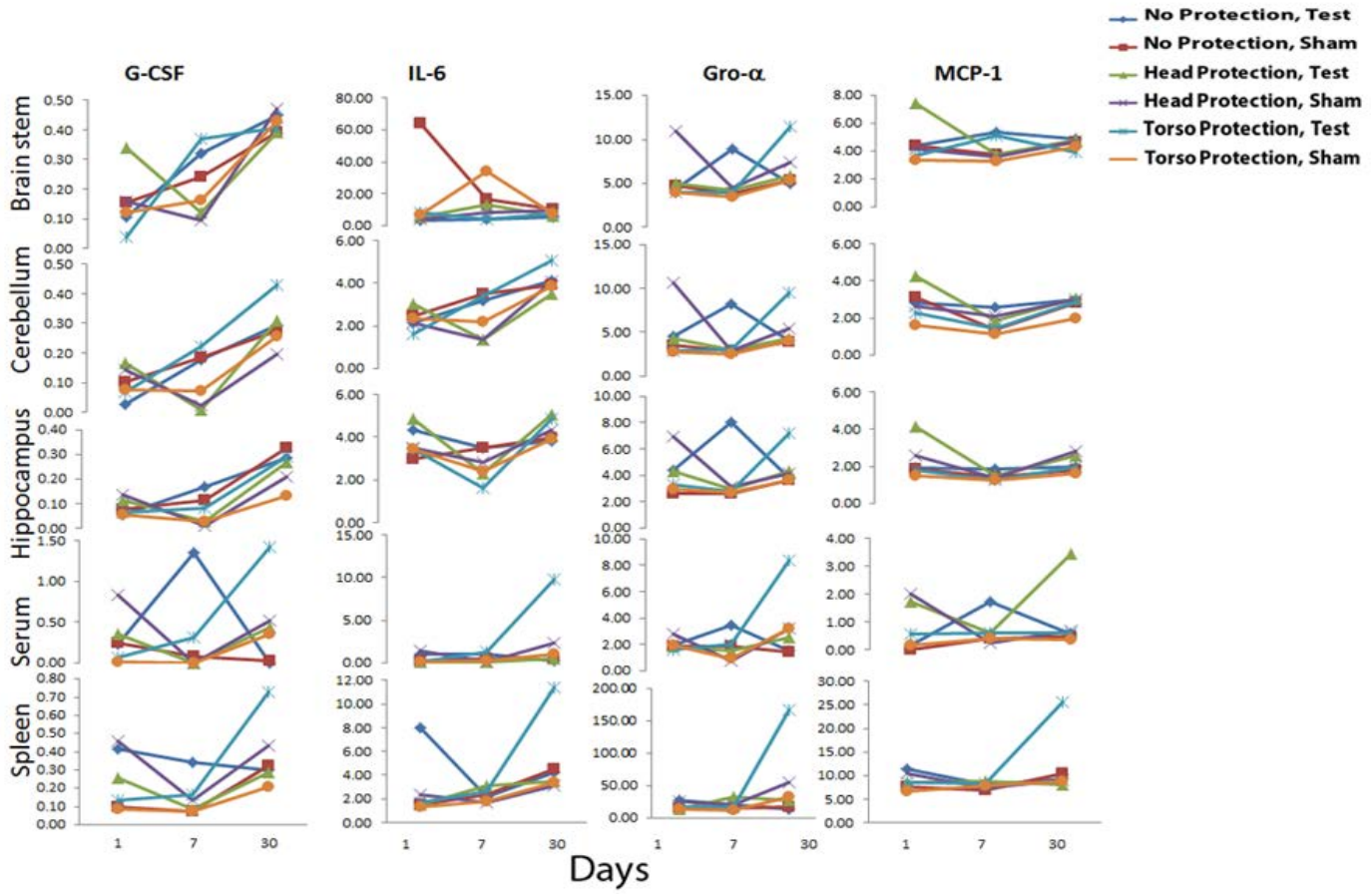

Figure 24 Temporal protein expression levels of G-CSF, IL-6, Gro-α, and MCP-1 in mice with and without protective wear and exposure to blast. Individual sample types are plotted in rows brain stem, cerebellum, hippocampus, serum, and spleen). The time post injury is plotted on the x-axis (1, 7, and 30 days post-blast). These plots depict the evolving data over the 30-day period. The y-axis represents the concentration in pg/ml.

Interestingly, the chemokines (G-CSF, Gro-α, and MCP-1) all appear upregulated in serum and spleen in the blast exposed torso protected group. IL-6, an interleukin that is induced by Gro-α, is also upregulated in these samples. Gro-α is upegulated in brain as well at 30 days post-injury.

<u>Aim IV (24 months – October 1, 2011 to September 30, 2013)</u> includes continuous correlation of imaging findings, molecular analyses, and functional data and further fine-tuning of the imaging modalities based on the validation results and correlations with outcome data.

$MnCl_2$-T1 MRI Normalization and Quantification

Phantom Development. Internal $MnCl_2$ controls (aka phantoms) were developed to allow normalization and quantification of $MnCl_2$-T1 MRI. Phantom Baseline data has been taken at various concentrations of MnCl2 in solution (Figure 25). Concentrations of $MnCl_2$ in H2O were 0, 0.01, 0.02, 0.5, 1 and 2 millimolar (mM). The concentrations were designed such that running lower and higher doses is not needed since water (H2O) is zero and 1 mM is already higher than injectate / animal mass (i.e. physiological dose). Even though correlation time and other phenomena are responsible for the curves behavior (Intensity versus concentration is graphed,

given that there are 4 points (between 0 and 0.5mM and they were repeated three times inside the coil for reliability), in the range of physiologically possible concentrations (injectate is 1mM and this must mix with blood pool and distribute throughout the body) a more or less linear response of concentration versus intensity is evident. Hence it is believed that any noted intensity in an MRI can be linearly associated with concentration up-take of MnCl2. Phantoms of 0.02 mM are placed above the head in the head rf-coil in every scan for calibration purposes and for concentration quantification purposes.

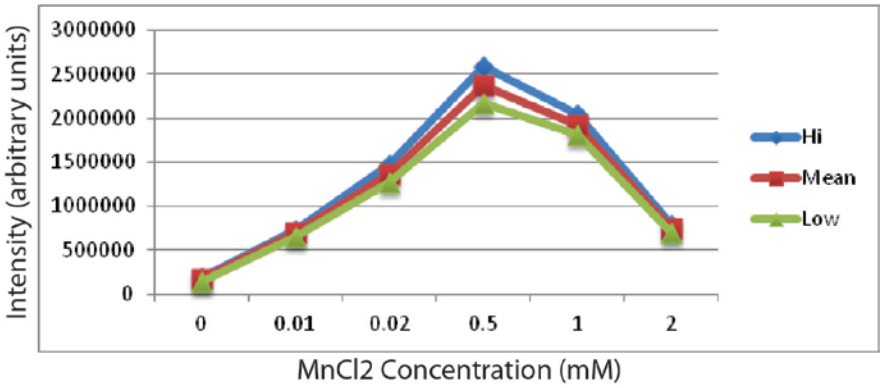

Figure 25. Phantom Intensity versus $MnCl_2$ Concentration

Normalization with Phantom. $MnCl_2$-enhanced MR imaging of TBI mouse brains was performed in conjunction with a 0.02mM MnCl2 phantom affixed to the brain coil in order to correct for variations in MRI homogeneity and imaging performance. Daily variations in phantom contrast were quantified with Paravision 5.0 Processing Software (fig. 26).

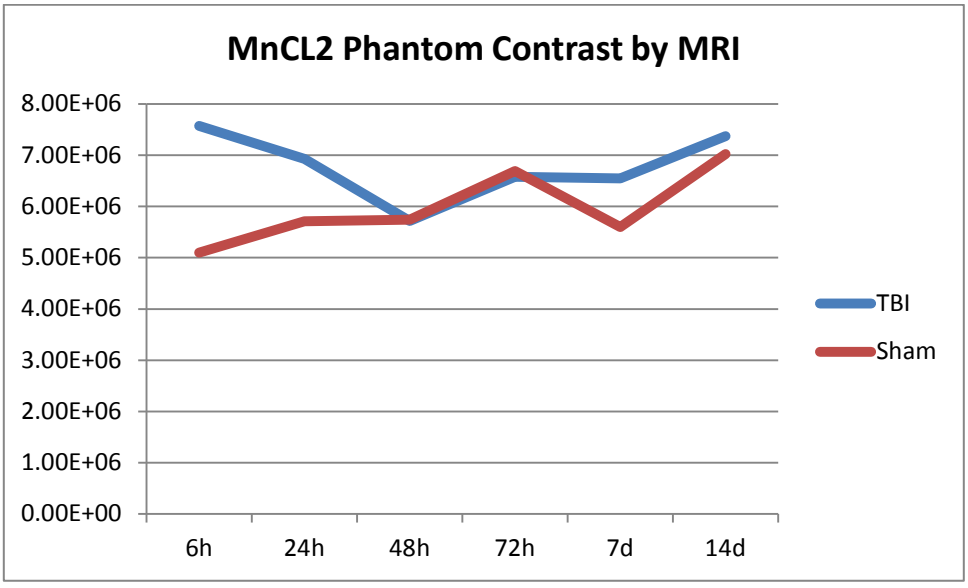

Figure 26 . Day-to-day variations in phantom contrast.

Normalization of $MnCl_2$-contrast enhancement of brain after TBI resulted in a more accurate measure of CNS uptake. These calculations are ongoing.

Optimization of $MnCl_2$ injection protocol for improved signal enhancement

So far, our $MnCl_2$-MRI studies have been performed by injection of $MnCl_2$ 24h **before** injury induction. This has resulted in a differential uptake of the contrast agent by the brain when comparing mice that have undergone TBI vs shams. However, although this uptake is quantifiable, it is subtle. It is known that TBI causes an impact in the neuronal homeostasis of calcium and that $MnCl_2$ is taken up by neuronal cells through Ca2+ voltage-gated channels. We therefore predicted that if $MnCl_2$ is made available to the brain immediately after injury-induction, uptake of $MnCl_2$ would increase due to the effect of the injury on these calcium channels and therefore, contrast-enhancement of the brain will be more obviously visible and quantifiable by MRI.

A set of seven mice (TBI and sham controls) were tested with the new conditions in October, 2012 (fig. 27). Following injury-induction, 100ul of a 100mM solution of MnCl2 was injected IP immediately **after** TBI (in contrast to prior experiments when agent had been injected before blast). MR imaging was performed longitudinally during 28days. MRI at 6h post-TBI showed a marked positive contrast in ventricles and peri-ventricular areas. At 24h, positive contrast was disseminated throughout the brain and lingered for several days.

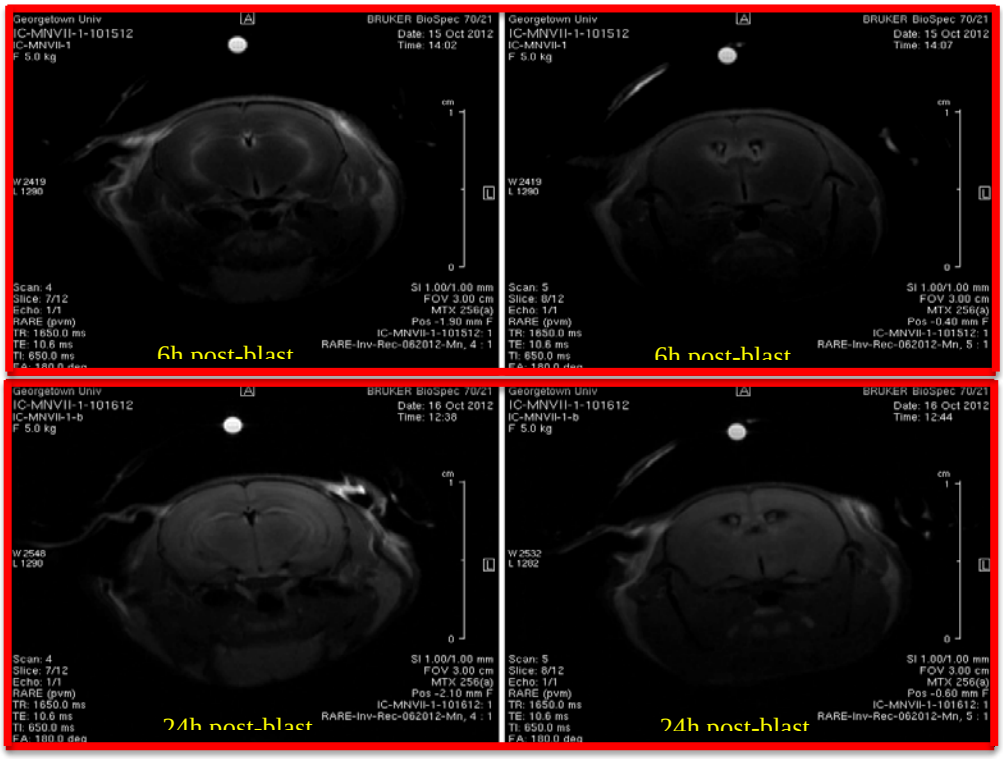

Figure 27. MnCl2-MRI in blast exposed animals. MnCl2 was injected immediately after blast exposure. The white circle above the brain is the phantom used for normalization.

In contrast, MR images of sham mice did not show this enhancement (fig. 28).

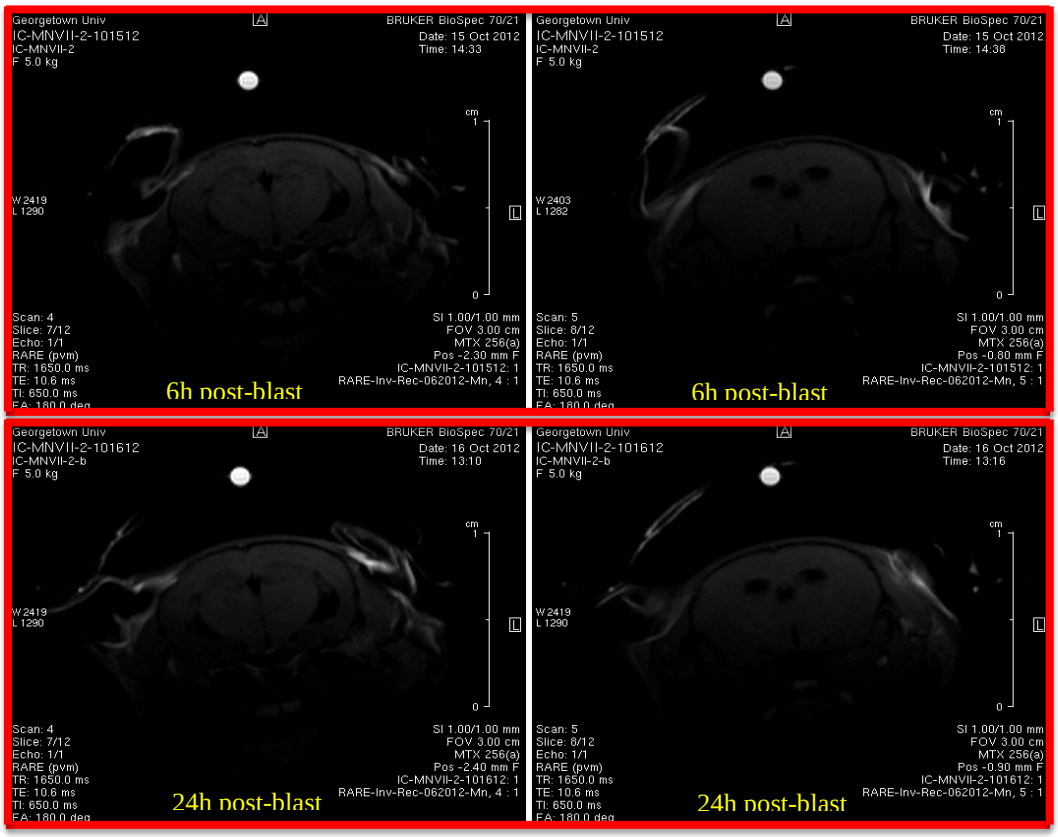

Figure 28. MnCl2-MRI in sham control animals. MnCl2 was injected immediately after blast exposure. The white circle above the brain is the phantom used for normalization.

Unfortunately, BINT followed by immediate $MnCl_2$ injection caused the animals to appear sickly and several died 24 to 72 hours after blast.

In November, 2012, the experiment was repeated under the same conditions and confirmed the enhanced differential in contrast uptake between blast exposed and sham mice.

To avoid death of mice by $MnCl_2$ toxicity, the experiment was repeated in December, 2012 with half of the dose of contrast agent (50ul of a 100mM solution of $MnCl_2$**)**. The lower dose resulted in similar differential uptake of $MnCl_2$ by BINT vs sham brains.

Quantification of contrast in specific areas of the brain using measurements normalized to the $MnCl_2$ phantom

Starting at 24 hours, the contrast was markedly increased in all areas of the brain in BINT mice in contrast to shams (Figs. 29-30).

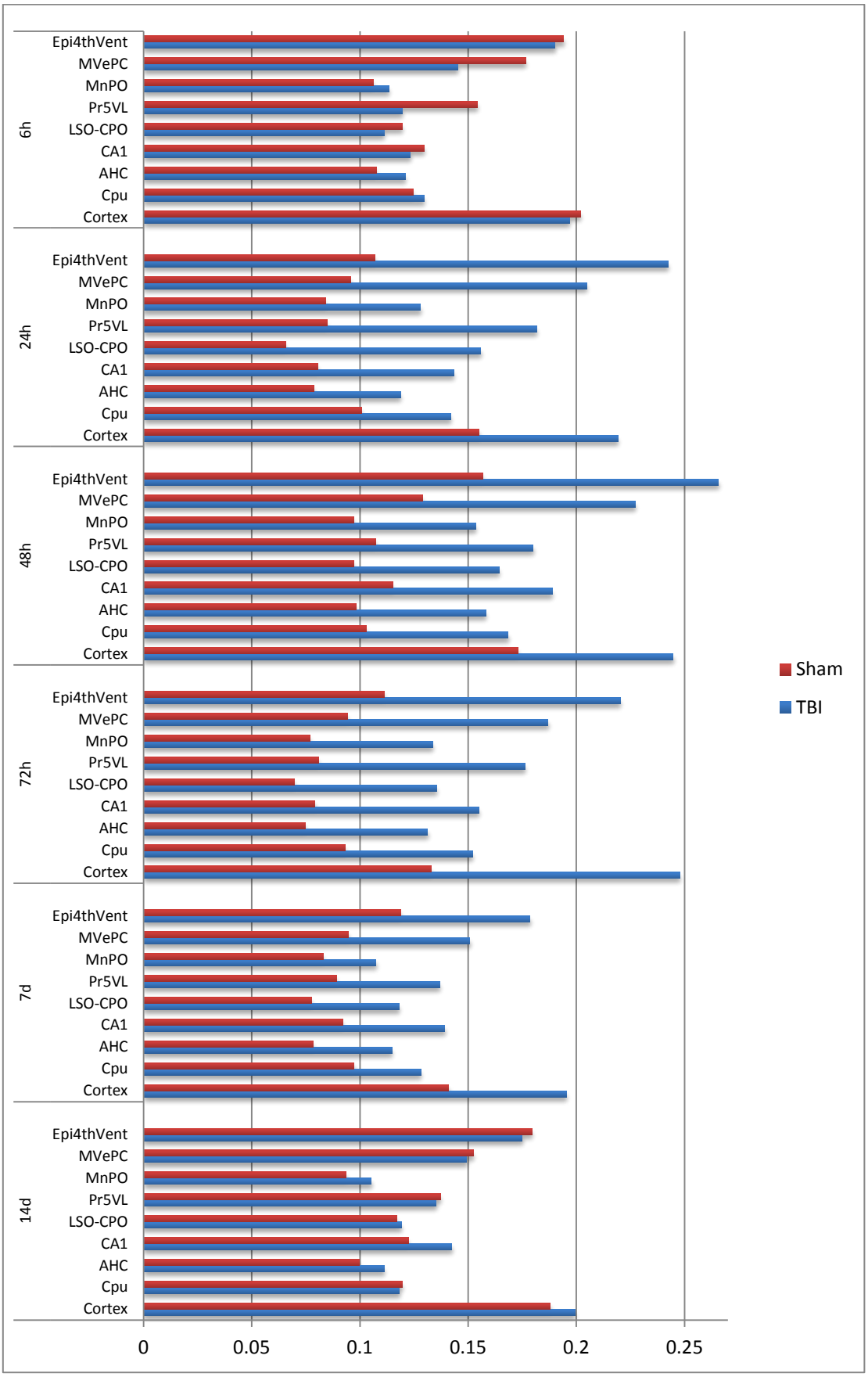

Figure 29. Temporal Profile of MnCl2-MRI enhancement in selected brain regions.

This difference in contrast continued for 7 days. By 14 days, there was no difference in $MnCl_2$ contrast enhancement between BINT and sham mice.

Figure 30. MnCl2-MRI plots with individual brain regions broken out. Plots show normalized intensity (arbitrary units) over a period of two weeks.

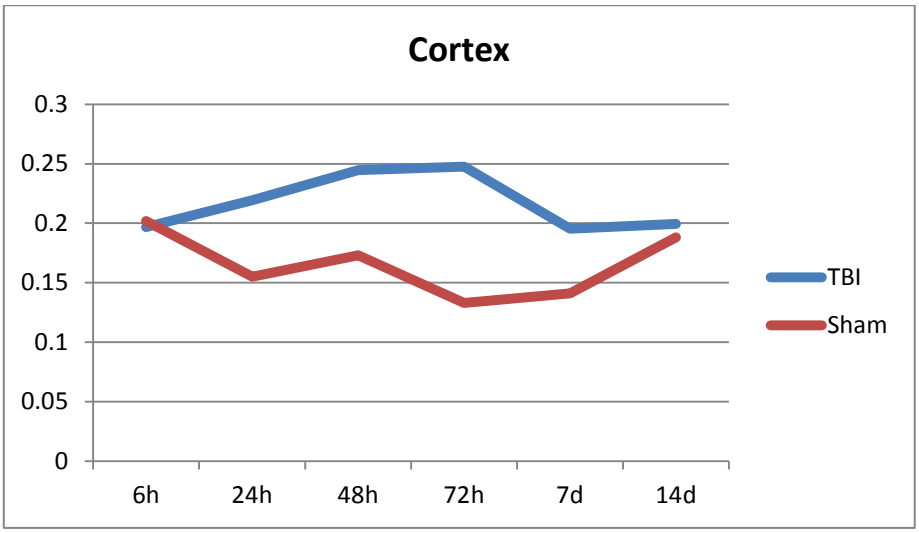

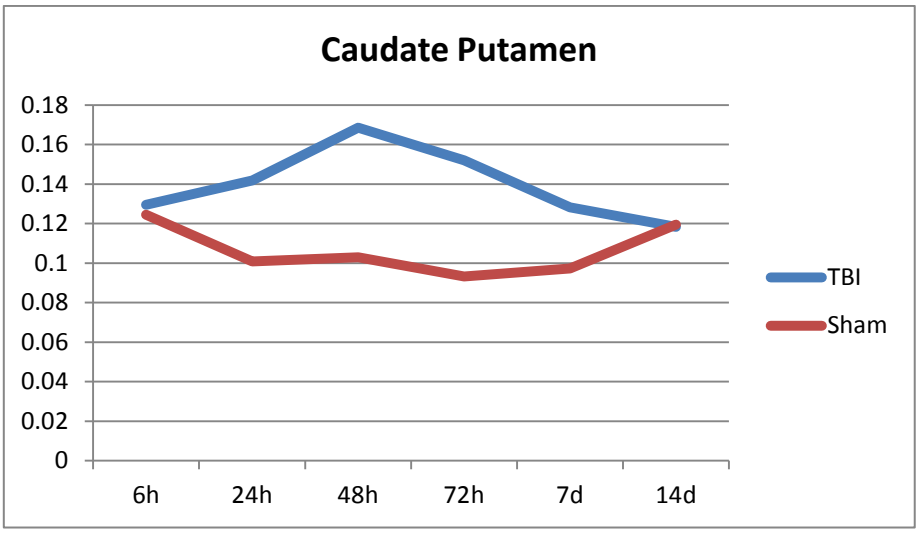

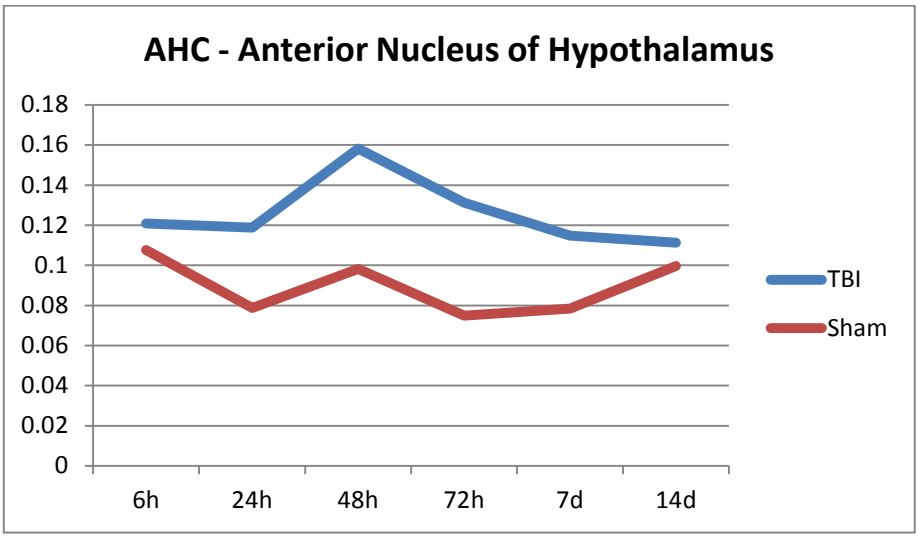
AHC - Anterior Nucleus of Hypothalamus
0.18
0.16
0.14
0.12
0.1
0.08
0.06
0.04
0.02
0
6h
24h
48h
72h
7d
14d
TBI
Sham

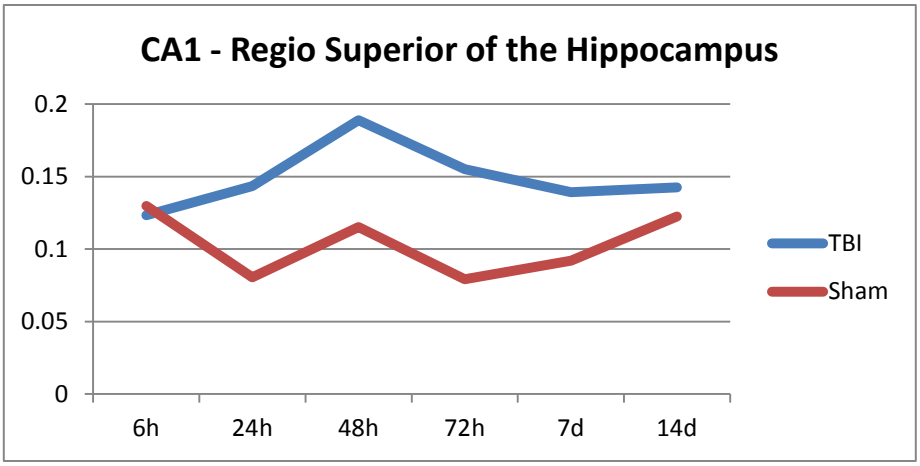
CA1 - Regio Superior of the Hippocampus
0.2
0.15
0.1
0.05
0
6h
24h
48h
72h
7d
14d
TBI
Sham

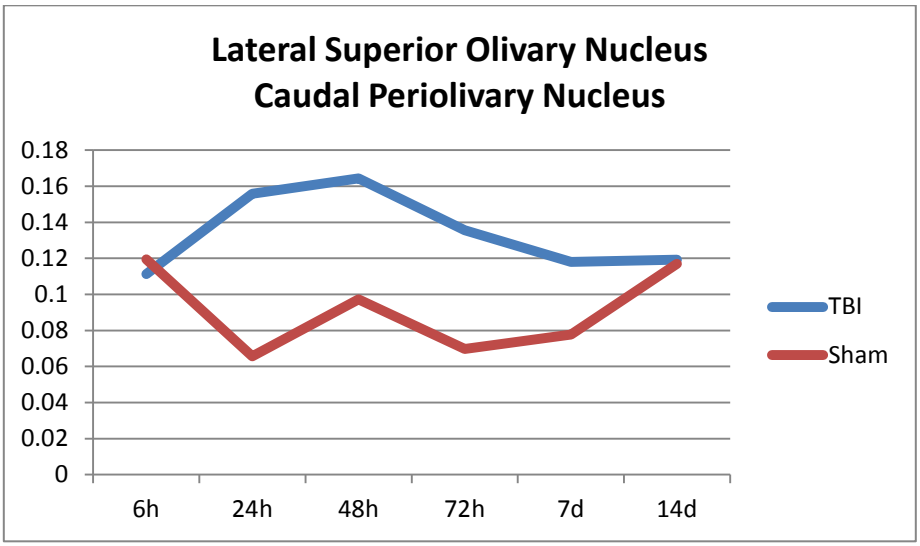
Lateral Superior Olivary Nucleus
Caudal Periolivary Nucleus
0.18
0.16
0.14
0.12
0.1
0.08
0.06
0.04
0.02
0
6h
24h
48h
72h
7d
14d
TBI
Sham

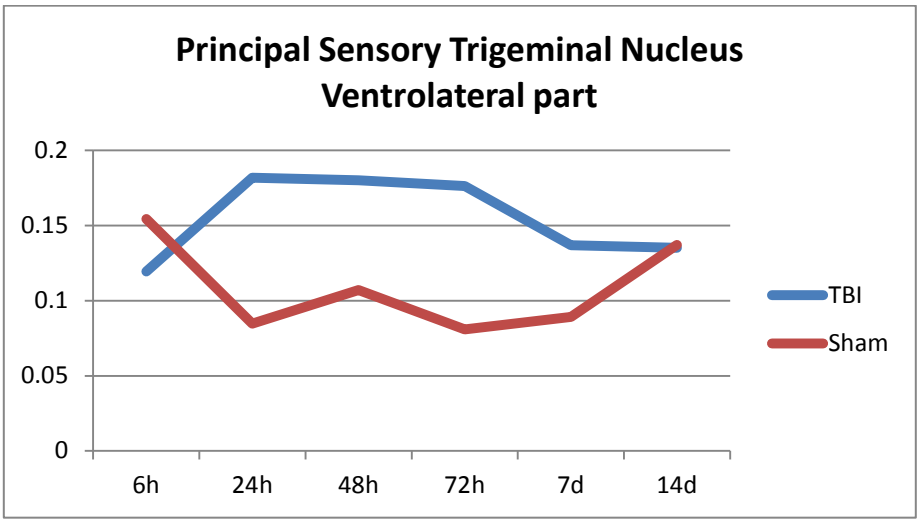
Principal Sensory Trigeminal Nucleus
Ventrolateral part
0.2
0.15
0.1
0.05
0
6h
24h
48h
72h
7d
14d
TBI
Sham

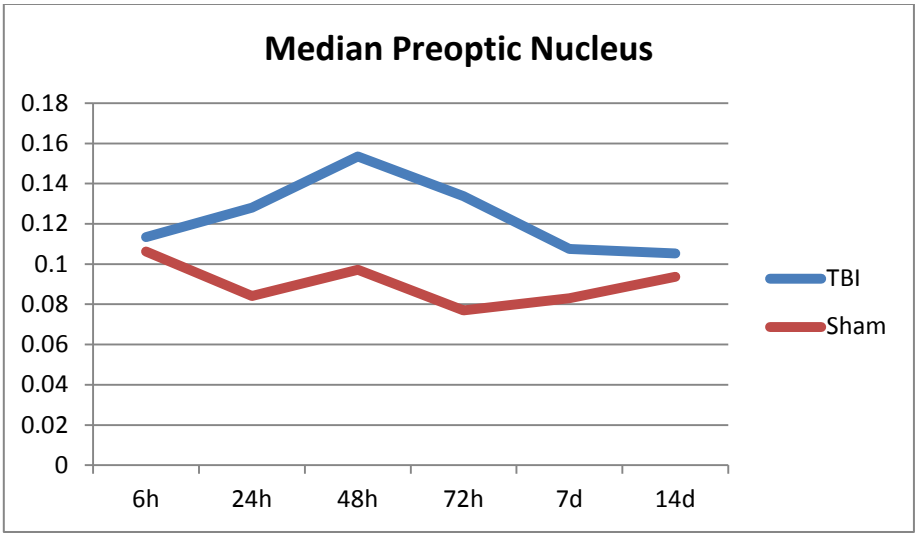
Median Preoptic Nucleus
0.18
0.16
0.14
0.12
0.1
0.08
0.06
0.04
0.02
0
6h
24h
48h
72h
7d
14d
TBI
Sham

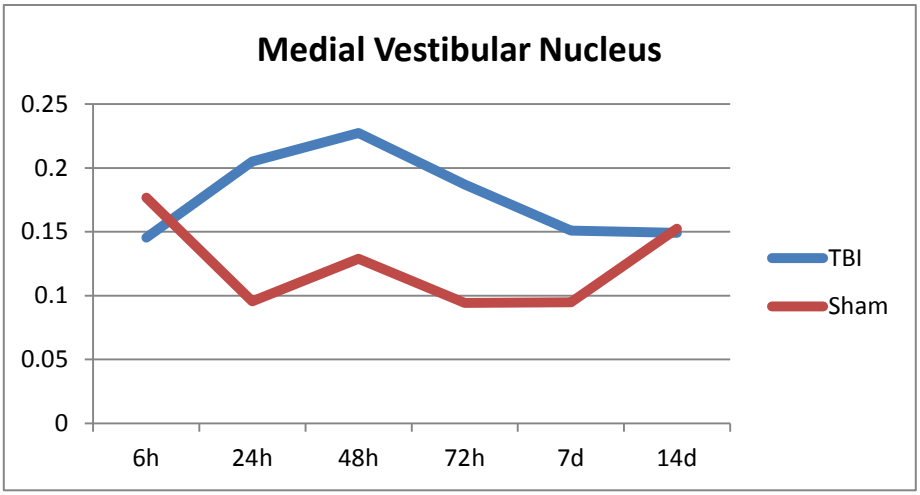
Medial Vestibular Nucleus
0.25
0.2
0.15
0.1
0.05
0
6h
24h
48h
72h
7d
14d
TBI
Sham

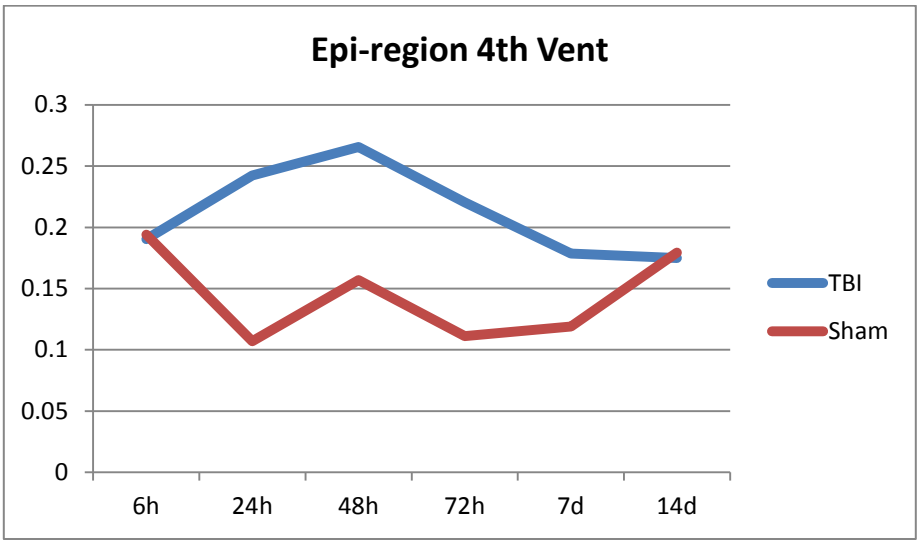

In conclusion, injection after injury-induction resulted in a prominent difference in the uptake of $MnCl_2$ by mouse brain between TBI mice vs shams in all regions sampled.

Aim 3 (24 months – October 1, 2011 to March 31, 2013) Characterization of functional outcomes in mice exposed to blast.

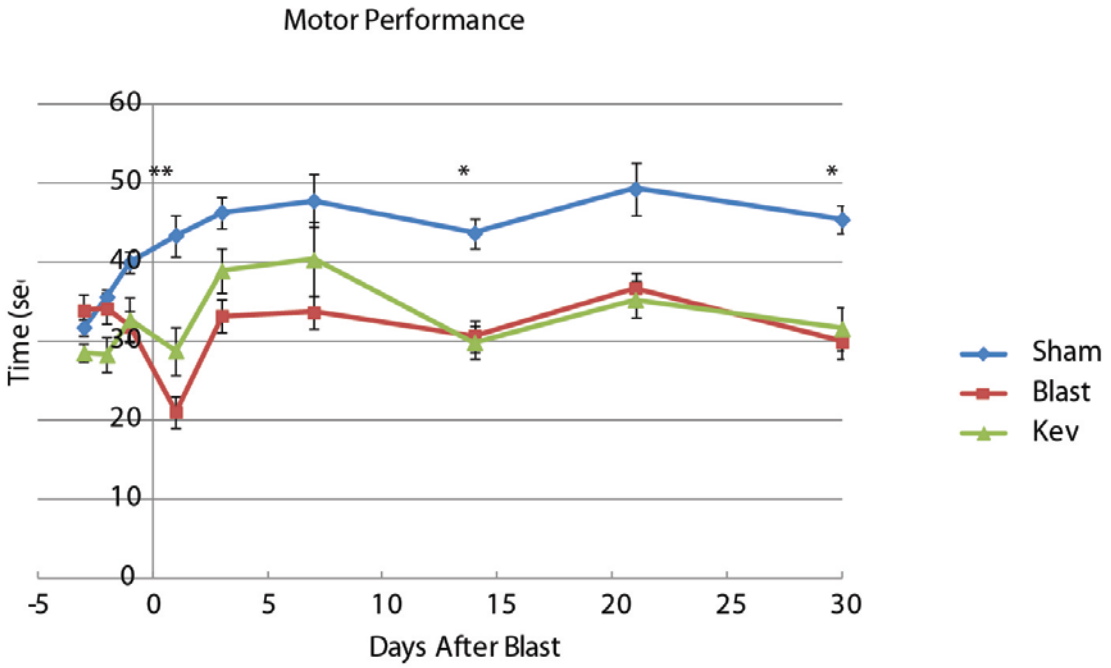

Figure 31 Motor performance in GFAP-luciferase transgenic animals exposed to mild/moderate blast with and without the surrogate outer tactical vest and sham controls. The results are shown as ± SE and measured over a 30-day post-injury period. (Unprotected blast exposed animals. N=12; Outer tactical vest animals (Kev) N=5; Sham N=8). Rotarod assessed motor outcomes in pre-trained mice. Motor performance was significantly decreased at two weeks and 30 days post trauma in unprotected and protected mice. One asterisk, $P<0.05$; two asterisks, $p<0.01$.

As had been demonstrated previously in C57Bl6 mice in Cernak et al we are also detecting motor impairment in the GFAP-luciferase transgenic animals (FVB/N-Tg(GFAP-luc)-Xen strain) that had been used in the in vivo GFAP imaging study(Cernak, Merkle et al. 2011).

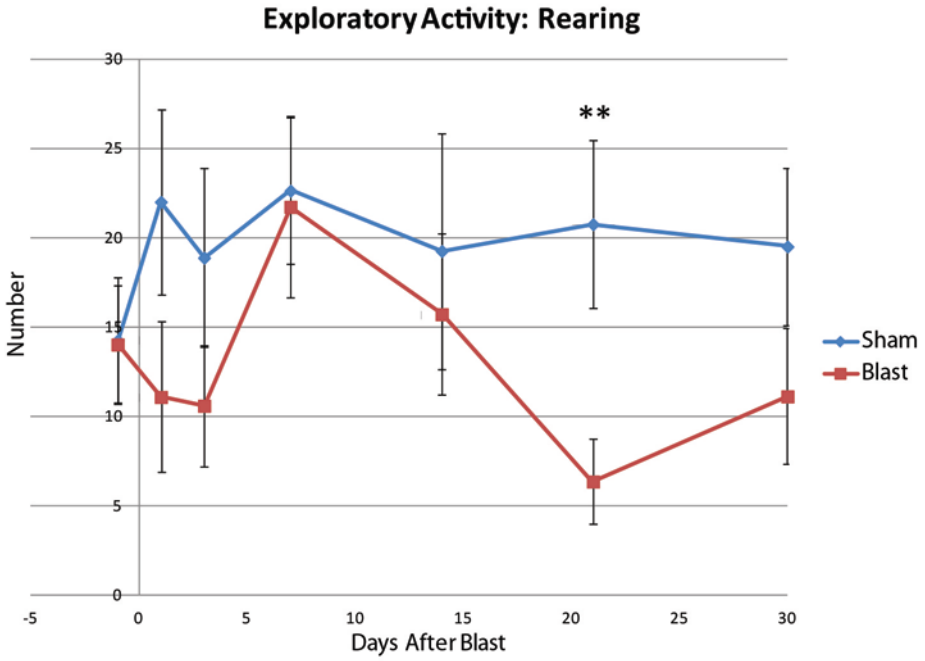

Figure 32 Exploratory activity in GFAP-luciferase transgenic animals exposed to mild/moderate blast and sham controls. The results are shown as ± SE and measured over a 30-day post-injury period. (blast exposed animals, N=12; Sham N=8). Rearing was significantly decreased at three weeks in post trauma mice. One asterisk, $P<0.05$; two asterisk, $p<0.01$.

As had been demonstrated previously in C57Bl6 mice in Cernak et al we are also detecting rearing impairment in the GFAP-luciferase transgenic animals (FVB/N-Tg(GFAP-luc)-Xen strain) (Cernak, Merkle et al. 2011).

We did not see a significant difference in distance traveled, freezing behavior (time immobile), or memory performance (shuttle box active avoidance assay) as had been demonstrated previously (Cernak, Merkle et al. 2011) but perhaps we would need to increase the number of animals to see this outcome (data not shown).

Future work:

Histology

- More subjects will be recruited to make statistical analysis possible.
- To better understand the nature of the microglial neuroinfammatory response, a series of sections will be prepared from each subject and processed for immunoperoxidase-DAB for markers of microglia of different functional states (resting, dividing, phagocytic, neurotoxic) including $K_V1.3$, $K_V.1.5$, p38 MAPK and PCNA.

- Wherever possible (i.e., in the optic tract and superior colliculus), cell counts will be performed with stereological methodologies. Cases will be grouped by experimental history and variance among groups will be statistically evaluated, including the use of appropriate post hoc testing.

Immunoprofiling

- More subjects (*n*= 3 per group with replicates in each group) will be recruited to make statistical analysis possible on the cytokine and chemokine expression analysis.
- Select markers will be further evaluated for expression levels.

MRI Imaging

- Complete imaging protocols to fill-in missing data.
- Continue to perform image intensity correction and plot normalized regions of interest.
- Include histology on imaged animals.

Key Accomplishments:

Histology

- A near complete set of brains has been collected for histology consisting of time points 1, 3, 7, 14, and 30 days post blast.
- Immunostaining and quantification for inflammation related markers (e.g. CD68, IbaI, and GFAP) has begun. Significant signal is detected in the visual pathway (i.e. optic tract, superior colliculus) and cerebellum.

Immunoprofiling

- Using multiplex analysis we analyzed protein expression for the following markers (i.e. Gro-α, G-CSF, IL-β, IL-10, IL-6, TNF-α, VEGF-A, IL-2, MCP-1) in different brain regions, serum, and spleen over a period of 30-days. Some interesting differences between torso shielded animals and other groups were noted that suggest chronic alterations in chemokines in the spleen, serum and the brain in torso protected animals.

MRI Imaging

- >100 MRI image sets were acquired to date.
- A phantom mimicking physiologically relevant contrast agent concentrations has been put into place. The known concentration phantom is being compared to tissue intensity for the quantification of contrast agent up-take in brain tissue.
- GUMC has setup new MRI hardware that appears to allow imaging of previously not-realizable aims.
- Optimization of $MnCl_2$ enhanced MRI has yielded robust signal differences globally throughout the brain between BINT and sham mice.

Functional Outcome

- A set of mild/moderate blast exposed GFAP-luciferase transgenic animals (FVB/N-Tg(GFAP-luc)-Xen strain) and shams were tested in rotarod, open field, and active avoidance tasks. These animals are exhibiting the same trends as previously reported (Cernak, Merkle et al. 2011). No difference was detected between C57BL6J animals wearing a surrogate outer tactical vest (OTV) and those which were unprotected.

Reportable outcomes

- Currently preparing a draft of the GFAP-luciferase IVIS imaging and functional analysis. Tentatively titled "Analysis on Neurological Outcome in Mice with Traumatic Brain Injury".
- Ongoing quantification and preparation of a manuscript describing the MnCl2-enhanced MR imaging results.

Conclusions

We have continued to amass results in support the hypothesis that there is a significant systemic influence in blast-induced neurotrauma. MRI imaging studies support the hypothesis that there is significant reactive gliosis at after blast injury. Histology is showing unique temporal and spatial patterns of activated microglia in the brain after blast injury. Immunoassays are revealing temporal differences in expression of cytokines and chemokines in the blood, brain, and spleen. Interestingly, we see some significant differences in expression of CXCL-1, G-CSF, IL-6 between torso shielded, head shielded, and no shield animals. This suggests an important neuroimmune interaction between the brain and systemic system.

Administrative

- Team review meeting was held at JHUAPL on September 4th. Attendees included Dr. Michele L. Schaefer (JHUAPL); Michael McLoughlin), deputy BAE (JHUAPL); Andrew Merkle, program manager (JHUAPL); Dr. Brock Wester (JHUAPL); Dr. Vassilis Koliatsos (JHUSOM); Dr. Leyan Xu (JHUSOM); Dr. Chris Albanese (GU); Dr. Olga Rodriguez (GU); and Dr. Stanley Fricke (CNMRC)
- Bi-weekly team telecons.
- Monthly reviews with Elaine Slujtner, financial manager.

References

Cernak, I. (2010). "The importance of systemic response in the pathobiology of blast-induced neurotrauma." Front Neurol **1**: 151.

Cernak, I., A. C. Merkle, et al. (2011). "The pathobiology of blast injuries and blast-induced neurotrauma as identified using a new experimental model of injury in mice." Neurobiol Dis **41**(2): 538-551.

Fagan, S. C., D. C. Hess, et al. (2004). "Targets for vascular protection after acute ischemic stroke." Stroke **35**(9): 2220-2225.

Jadhav, V., G. Matchett, et al. (2007). "Inhibition of Src tyrosine kinase and effect on outcomes in a new in vivo model of surgically induced brain injury." J Neurosurg **106**(4): 680-686.

Koliatsos, V. E., I. Cernak, et al. (2011). "A mouse model of blast injury to brain: initial pathological, neuropathological, and behavioral characterization." J Neuropathol Exp Neurol **70**(5): 399-416.

Lyons, A., Lynch, A.M. et al. (2009). "Fractalkine-induced activation of the phosphatidylinositol-3 kinase pathway attenuates microglial activation in vivo and in vitro." J Neurochem 110: 1547-1556.

Nag, S., M. R. Eskandarian, et al. (2002). "Differential expression of vascular endothelial growth factor-A (VEGF-A) and VEGF-B after brain injury." J Neuropathol Exp Neurol **61**(9): 778-788.

Nag, S., J. L. Takahashi, et al. (1997). "Role of vascular endothelial growth factor in blood-brain barrier breakdown and angiogenesis in brain trauma." J Neuropathol Exp Neurol **56**(8): 912-921.

Owens, B. D., J. F. Kragh, Jr., et al. (2008). "Combat wounds in operation Iraqi Freedom and operation Enduring Freedom." J Trauma **64**(2): 295-299.

Sheng, J. G., S. H. Bora, et al. (2003). "Lipopolysaccharide-induced-neuroinflammation increases intracellular accumulation of amyloid precursor protein and amyloid beta peptide in APPswe transgenic mice." Neurobiol Dis **14**(1): 133-145.

Zhang, Z. G., L. Zhang, et al. (2000). "VEGF enhances angiogenesis and promotes blood-brain barrier leakage in the ischemic brain." J Clin Invest **106**(7): 829-838.